

RESEARCH ARTICLE

Novel derivative of Paeonol, Paeononlsilatie sodium, alleviates behavioral damage and hippocampal dendritic injury in Alzheimer's disease concurrent with cofilin1/phosphorylated-cofilin1 and RAC1/CDC42 alterations in rats



Fei Han¹, Ting-Ting Zhuang¹, Jing-Jing Chen¹, Xiu-Ling Zhu^{1,2}, Ya-Fei Cai¹, Ya-Ping Lu^{1*}

1 College of Life Science, Anhui Normal University, Wuhu, China, **2** Department of Anatomy, Wannan Medical College, Wuhu, China

* yapinglu@ahnu.edu.cn

OPEN ACCESS

Citation: Han F, Zhuang T-T, Chen J-J, Zhu X-L, Cai Y-F, Lu Y-P (2017) Novel derivative of Paeonol, Paeononlsilatie sodium, alleviates behavioral damage and hippocampal dendritic injury in Alzheimer's disease concurrent with cofilin1/phosphorylated-cofilin1 and RAC1/CDC42 alterations in rats. PLoS ONE 12(9): e0185102. <https://doi.org/10.1371/journal.pone.0185102>

Editor: Ferdinando Di Cunto, Università degli Studi di Torino, ITALY

Received: June 21, 2017

Accepted: September 6, 2017

Published: September 21, 2017

Copyright: © 2017 Han et al. This is an open access article distributed under the terms of the [Creative Commons Attribution License](#), which permits unrestricted use, distribution, and reproduction in any medium, provided the original author and source are credited.

Data Availability Statement: All relevant data are within the paper and its Supporting Information files.

Funding: The present study was supported by National Natural Science Foundation of China (No. 30470537), Natural Science Foundation of Department of Education, Anhui Province (ZD2008006-1), Innovation Team of Scientific Research Platform in Anhui Universities, and

Abstract

Alzheimer's disease (AD) is a typical hippocampal amnesia and the most common senile dementia. Many studies suggest that cognitive impairments are more closely correlated with synaptic loss than the burden of amyloid deposits in AD progression. To date, there is no effective treatment for this disease. Paeonol has been widely employed in traditional Chinese medicine. This compound improves learning behavior in an animal model; however, the mechanism remains unclear. In this study, Paeononlsilatie sodium (Pa), a derivative of Paeonol, attenuated *D*-galactose (*D*-gal) and AlCl₃-induced behavioral damages in rats based on evaluations of the open field test (OFT), elevated plus maze test (EPMT), and Morris water maze test (MWMT). Pa increased the dendritic complexity and the density of dendritic spines. Correlation analysis indicated that morphological changes in neuronal dendrites are closely correlated with behavioral changes. Pa treatment reduced the production of Aβ, affected the phosphorylation and redistribution of cofilin1 and inhibited rod-like formation in hippocampal neurons. The induction of *D*-gal and AlCl₃ promoted the expression of RAC1/CDC42 expression; however, the tendency of gene expression was inhibited by pre-treatment with Pa. Taken together, our results suggest that Pa may represent a novel therapeutic agent for the improvement of cognitive and emotional behaviors and dendritic morphology in an AD animal model.

Introduction

Alzheimer's disease (AD) is the most common form of elderly dementia and has been generally regarded as an amnesic syndrome of hippocampal type, which represents the most important clinic feature for the diagnosis of typical AD [1, 2] and accounts for 50%–60% of all

Provincial Key Laboratory of Biotic Environment and Ecological Safety in Anhui. The funders had no role in study design, data collection and analysis, decision to publish, or preparation of the manuscript.

Competing interests: The authors have declared that no competing interests exist.

dementia cases [3]. In the Western world, the percentage of AD dementias is less than 1% in individuals aged 60–64 years, whereas it is approximately 24% to 33% in individuals aged 85 years or older [3]. Globally, more than 40 million individuals over 60 years have been estimated to have AD dementia, and the number of patients will double every 20 years until at least 2050 [4, 5].

The marked pathological features of AD include the formations of extracellular senile plaques from abnormally folded A β s and intracellular neurofibrillary tangles from hyperphosphorylated tau proteins [6]. A β is considered the trigger in the disease process [7–10]; however, it is also a controversial marker [11]. The oligomers of A β , particularly soluble oligomers, such as “A β -Derived Diffusible Ligands” (ADDLs), which are mainly trimeric to 12meric A β_{1-42} -oligomers, are considered to be the most cytotoxic forms [12–14]. These oligomers play an essential role during the occurrence and development of AD [13–15].

Dendritic spines undertake an important role in information processing in the brain, particularly for excitatory synaptic transmission [16–18] and plasticity [19]. In AD pathogenesis, synaptic loss contributes to cognitive impairments more than the burden of amyloid plaques [20, 21]. Previous studies in clinical settings [22] and animal models of AD [23–25] have confirmed the significant decrease in the number and morphological changes in dendritic spines in the neocortex and hippocampus compared with age-matched controls [17].

A β oligomers bind to various membrane receptors [26], such as glutamate receptors [27–29] and LirrB2 (murine PirB) [30], and transmit signals to GTPase-mediated different pathways to affect the activation/deactivation of cofilin1 and the formation of cofilin-actin rods, which ultimately affects the synaptic transmission and survival of postsynaptic neurons [17, 19].

To date, there is no effective treatment for this disease [31]. Paeonol (2'-hydroxy-4'-methoxyacetophenone, C₉H₁₀O₃) is a phenolic acid compound extracted from the famous Cortex Moutan, which has been widely employed in traditional Chinese medicine (TCM). It is well established that Paeonol exerts anti-inflammatory activities to relieve ovalbumin-induced asthma [32] and cigarette smoke-induced lung inflammation [33] in a murine model, free-radical scavenging properties to prevent against neurotoxicity in vitro [34, 35], and anti-tumor effects in culture cells [36, 37]. Paeonol administration may reduce ischemia-reperfusion injured cerebral infarction [38] and ameliorate cognitive deficits in streptozotocin-induced diabetic rats [39].

Recent studies have indicated that Paeonol attenuates oxidative stress to protect against acetaminophen-induced hepatotoxicity in mice [40], reduces neuronal apoptosis in myocardial infarcted rats by inhibiting oxidative stress through the Nrf2-HO-1 and PI3K-Akt pathways [41], and alleviates cerebral ischemic injuries in mice by upregulating the expressions of pAkt, Nrf2, and HO-1 and ameliorating BBB permeability [42]; it also attenuates lipopolysaccharide-induced depressive-like behaviors in mice [43]. Paeonol applications improve Alzheimer's disease-like behaviors in a rat model [44]; however, the mechanism remains unclear. To reduce A β oligomers and develop a novel compound to treat AD, in this study, we used Paeonolnsilatie sodium (a derivative of Paeonol) to treat an AD animal model and investigated its potential mechanisms.

Experimental procedures

Drugs and chemicals

Paeonolnsilatie sodium injection (C₉H₉NaO₆S, a derivative of Paeonol, 0.1 g/2 ml), which has the same pharmacological effects as Paeonol and has been approved by the Chinese FDA for clinical use in the treatment of muscle pain, arthralgia, rheumatism, neuralgia and abdominal

pain (No. H20064790, <http://drugs.medlive.cn/drugref/html/18322.shtml>), was purchased from Jinling Pharmaceutical Company (Nanjing, China). *D*-gal was purchased from Sangon Biotech (Shanghai, China). AlCl₃ (Al) was purchased from Guangzhou Chemical Reagent Factory (Guangzhou, China). CDC42 and RAC1 antibodies were purchased from Boster Biological Technology Co., LTD (Wuhan, China). Phospho-Tau (Ser202) and Aβ_{1–42} antibodies (used to recognize the Aβ fibrils) were purchased from Bioss Biological Technology Co., LTD (Beijing, China). RHOA antibody was purchased from Sangon Biological Technology Co., LTD (Wuhan, China). A11 antibody (used to recognize the Aβ oligomers [45], SAB5200113) was purchased from Sigma-Aldrich (St. Louis, USA). Cofilin1 antibody and DAPI were purchased from Santa Cruz Biotechnology (Shanghai, China). Other chemicals were purchased from Sigma.

Ethical approval of the study

Adult male Sprague-Dawley (SD) rats (180–200 g) were obtained from Shandong Experimental Animal Center (license number: SCXK20140007; Jinan, China) and housed at 21 ± 2°C, with a light cycle between 08:00 h and 20:00 h. Food and water were provided *ad libitum*. Animals were treated according to the Guidelines of the Regulations of Experimental Animal Administration issued by the State Committee of Science and Technology of the People's Republic of China on November 14, 1988. All animal experiments were conducted with the approval of the Animal Use and Care Committee of Anhui Normal University (2015002).

Establishment of AD rat model

AlCl₃ and *D*-gal co-induced animal models may be used to characterize AD-like behavioral and pathological features, as well as pathologic processes without the genetic background of gene mutations and have thus been widely used in AD-related studies [46–54]. In this study, *D*-gal was dissolved in physiologic saline (0.9%) and injected (100 mg/kg/day, once per day, s.c.). AlCl₃ was dissolved in double-distilled water (DDW) and administered (40 mg/kg/day, once per day, i.g.). Model induction lasted for 42 days.

Group and treatment

Following a one-week adaptation period, the rats were randomly divided into the control group (CG), *D*-gal + AlCl₃ group (DA group treated with *D*-gal + AlCl₃ for 42 days), Pa treatment group (50 mg/kg, i.p., 1 hour before treatment with AlCl₃ + *D*-gal) for 2 weeks (Pa2 group treated with AlCl₃ + *D*-gal + saline water (pretreatment) for 28 days, followed by AlCl₃ + *D*-gal + Pa for 14 days), and Pa treatment group for 6 weeks (Pa6 group treated with AlCl₃ + *D*-gal + Pa for 42 days). The induction of CG and the pretreatments for CG or DA were all volume-matched saline water.

Behavioral tests

OFT. The OFT was used to evaluate animal locomotor activity and emotional response [55]. The apparatus was opaque and black all around, including a square 80 cm × 80 cm surrounded by a height of 40 cm walls, and the bottom was divided into 25 quadrates of 16 cm × 16 cm by a white line. In a quiet environment, each rat was placed in the center area, which was defined as 9 squares in the center, and the behaviors were recorded for 5 min. The device was cleaned with 70% ethanol thoroughly after each trial. The number of squares crossed, number of clean movements, and number of rears were recorded. The animals were

placed in the laboratory room 30 min prior to testing to adapt to the environment. The observers were blind to the rats of the different treatment groups.

EPMT. The EPMT has typically been used to evaluate anxiety behaviors [56]. The apparatus consisted of four black arms (50 cm×10 cm) and a central square platform (10 cm×10 cm). Two of the arms were closed arms with walls (40 cm height), and the other two arms were open without walls. The maze was elevated 50 cm from the floor. The rats were placed onto the center platform of the maze facing an open arm, and their activities were recorded for 5 minutes. When a rat placed its four paws into an arm, it was counted as entry in the arm. The maze was cleaned with 70% ethanol thoroughly after each trial. The following parameters were recorded: the time spent in the open arms, the time spent in the closed arms, and the number of head dipping. The experimenters who recorded the data were unaware of the grouping.

MWMT. Spatial learning and memory capability were assessed using a modified MWMT. The pool (1.5 m in diameter, 50 cm in height) was filled with water to a depth of 30 cm. A circular escape platform (15 cm in diameter) was submerged 2 cm below the water surface. The water was clouded with black food coloring to prevent the visual image of the submerged platform. On the last five days during treatment for each group, the rats were trained to find a concealed platform in the MWM for five consecutive days. The MWM test was conducted according to previously described methods [57]. Briefly, the acquisition phase comprised four trials per day in which the animals learned to find the concealed platform. The rats were placed facing the wall at one of four designated start points in each trial. Each rat was allowed to find the platform for 60 s and remained on the platform for 20 s. If the rat could not reach the platform within 60 s, it was gently guided to the platform and remained for 20 s, and the results (time taken to find the platform) were recorded as 60 s. The average escape latencies of the four trials per day were used for statistical analysis. A longer time spent in finding the platform was used to assess the extent of learning impairment.

Twenty-four hours after the final acquisition trial, a single 60 s probe task was tested following the removal of the platform from the pool. The probe trials were recorded with a video camera to calculate the time the rats spent in the target quadrant. The longer the rat remained in the target quadrant, the better it scored for spatial memory. The time was manually recorded with a stopwatch (precision 1/100 seconds) by two observers, who were blind to the rats of the different treatment groups.

Tissue preparation

Following the behavioral tests, the rats were deeply anesthetized with 1% carbitral and perfused (via a transcardial approach) with 0.9% saline followed by 1) euthanasia via decapitation and isolation of hippocampal tissue from the brain, half of which was stored in Golgi-cox solution, while the other half of the hippocampus was stored in a -80°C refrigerator for further Western blot analysis; 2) perfusion with 4% paraformaldehyde and euthanasia, followed by the hippocampal tissues being collected and embedded in paraffin wax. The paraffin-embedded tissues were cut with a Leica microtome (RM2235) into serial coronal sections (6 µm).

Golgi-Cox staining

The Golgi–Cox technique was mainly conducted as described in the literature [58]. In brief, brain tissues were stored in Golgi-Cox solution in the dark at 37°C for 48 h and subsequently sectioned (200 µm thick coronal sections) using a vibratome (NVSL/NVSLM1). The sections were then immersed in alcohol (50%) for 5 min, ammonium hydroxide for 5–10 min, and 5% sodium thiosulfate in the dark for 10 min and serially dehydrated in solute alcohol, including 70%, 80%, and 95% alcohol (7 min × 2 for each) and 99% 1-butanol for 7 min; the samples

were subsequently cleaned in xylene for 5 min and medium mounted with coverslips using Rhamsan gum.

Immunohistochemistry and immunofluorescence

After being deparaffinized and rehydrated, the sections were treated with 0.3% hydrogen peroxide in phosphate buffered solution (PBS, pH 7.0) that contained 0.3% Triton X-100 for 30 min. The sections were subsequently treated twice (2×10 min) by microwaves (700 W) in 0.05 M citrate buffered saline (pH 6.0). After being washed in PBS, the sections were blocked with normal bovine serum in PBS for 1 h at 37°C, followed by incubation with primary antibodies [rabbit A β_{1-42} pA (1:200), rabbit phospho-tau (p-tau) pA (1:200) or mouse cofilin1 mA (1:200)] overnight at 4°C. Single labeling with DAB (A β_{1-42} and p-tau immunoreactivity): after being washed, the sections were incubated with the secondary antibody goat anti-rabbit (Boster Biotech, Wuhan, China) for 1 h at 37°C, which was performed as previously described [59]. Double labeling with fluorescein labeling methods previously described by our group [60]: after being washed, the sections were incubated with biotinylated horse anti-mouse IgG diluted in PBS (1:200) that contained 5% normal horse serum for 1 h and then incubated with CyTM3-labeled streptavidin (Kirkegaard and Perry Laboratories) diluted in PBS (1:500) for 30 min at room temperature, followed by incubation with 0.05 M glycine-HCl buffer saline (pH 2.2) for 2 h at room temperature to quench additional antibodies; the samples were subsequently incubated with second primary antibodies against rabbit p-cofilin1 pA (1:200) for 24 h at 4°C and incubated with the fluorescein isothiocyanate (FITC)-conjugated goat anti-rabbit IgG (Vector Laboratories, Burlingame, CA) for 1 h, diluted in PBS (1:100). Finally, the sections were coverslipped with glycerin. Control samples were simultaneously performed following the same procedures as the test samples with the exception that the primary antibodies were omitted.

Quantification of dendrites and spines

Quantitative methods of the dendritic branch and length have been previously described in the literatures [61, 62]. Briefly, the regions tested were determined at a low magnification according to Paxinos et al [63], and > 5 neurons in each hippocampal region per rat were selected to acquire their photographs, which were used for quantificational analysis. The criteria used to select neurons for quantitative analysis have been previously described [61, 64, 65]. Each selected neuron was analyzed using ImageJ software. Neuronal branches were traced by the Neuron J plug-in to count their total dendritic length, and dendritic intersections that cross the concentric circles were counted using the Sholl analysis plug-in protocol [65–67].

The analysis of the density and classification of dendritic spines were mainly based on the methods described in the previous literatures [61, 62]. Concisely, three independent coronal sections at the level of the lateral geniculate body per rat were used for analysis. At the apical proximal dendrites (< 50 μm from the center of the neuronal body), apical distal dendrites (> 150 μm from the center of neuronal body), and basal dendrites in CA1 and CA3, secondary or tertiary dendritic segments of pyramidal neurons were selected for analysis. In the DG, the apical dendritic segments at the outer 1/3 and 2/3 from the body of the granule neurons were selected for analysis. Z-stacks of Golgi-stained dendrites (up to 80 microns total on Z-axis; optical section thickness = 0.5 mm, i.e., 160 images per stack) were obtained at 60×6 magnification on an OLYMPUS FV1000. The Golgi spine images of the Z-stacks were analyzed using RECONSTRUCT software, which is freely available from <http://synapses.clm.utexas.edu>. The analysis was divided into three steps: step 1, series import and calibration; step 2, dendritic segment identification and measurement; and step 3, spine measurement and classification (S1 Fig).

Image analysis and quantification

Image analysis and quantification of the histological sections were performed by one author who was not aware of the experimental protocol. Images were captured under a microscope (BX51; Olympus, Tokyo, Japan) equipped with a DP70 digital camera or Laser scanning confocal microscope (OLYMPUS FV1000) and analyzed using image analysis software (ImageJ). In serial sections between Bregma -2.52 and -4.80 mm, one section was selected at intervals of every sixth section. The percentage of hippocampal regions covered by A β immunopositive regions was measured to estimate the A β burden [68]. The F-actin density was assessed by the percentage of phalloidin positive staining in different regions of the hippocampus.

Western blot analysis

For western immunoblot analysis, 10% (w/v) hippocampal homogenates were centrifuged at 12,000 $\times g$ for 30 min at 4°C, and the supernatants were transferred to clean tubes and stored as previously described [69]. The total protein concentration in the supernatants was determined using the Bicinchoninic acid assay (BCA; Pierce). Samples (40 μ g of total protein), mixed with an equal volume of Tricine sample buffer, were electrophoresed on various concentrations of Tris-tricine polyacrylamide gels (under nonreducing conditions) and transferred to nitrocellulose membranes. The blots were blocked with 5% nonfat dry milk in Tris-buffered saline Tween 20 (TBS-T) for 2 h at room temperature. RHOA (1:400), RAC1 (1:200), CDC42 (1:200), cofilin (1:100), p-cofilin (1:800), or A11 (1:800) antibodies were diluted in 0.1% BSA/TBS-T, covered with plastic wrap and incubated for 12 h at 4°C. Bound antibodies were visualized with horseradish peroxidase-conjugated secondary antibodies and the ECL detection system (BEYOTIME Biological Technology Co., LTD, China). Densitometric analysis of antibody specific bands was performed with NIH ImageJ version 1.34 software.

Statistical analyses

Analysis of variance (ANOVA) was used for comparisons of more than three groups, and a two-tailed *t* test was used for comparisons between two groups. The data of the spatial navigation tasks and the Sholl analysis were analyzed by a repeated ANOVA followed by post hoc Bonferroni's multiple comparisons. Other data were analyzed via one-way ANOVA followed by *post hoc* Least-significant difference (LSD). All data were analyzed with SPSS v21.0 software (IBM, New York, NY, USA) and expressed as the mean \pm standard error of the mean (SEM). $P < 0.05$ was considered to be statistically significant.

Results

Pa ameliorated *D*-gal and AlCl₃-induced behavioral damage

To determine the preventive effects of Pa on *D*-gal and AlCl₃-induced behavioral damage, rats were pre-treated with Pa (50 mg/kg) for 6 weeks. The OFT, EPMT and MWMT were employed to evaluate the animal behavioral performances. The OFT used in this study was represented by three parameters, including the number of squares crossed, the number of clean movements, and the number of rears. One-way ANOVA identified significant differences between the groups for these three parameters ($P < 0.001$ for all). Compared with the CG, the three parameters all showed significant decreases observed in DA ($P < 0.001$ for all). Pre-treatment with Pa significantly increased the number of squares ($P < 0.05$), the number of clean movements ($P < 0.05$), and the sum of rears ($P < 0.001$) in Pa6 compared with DA (Fig 1A–1C).

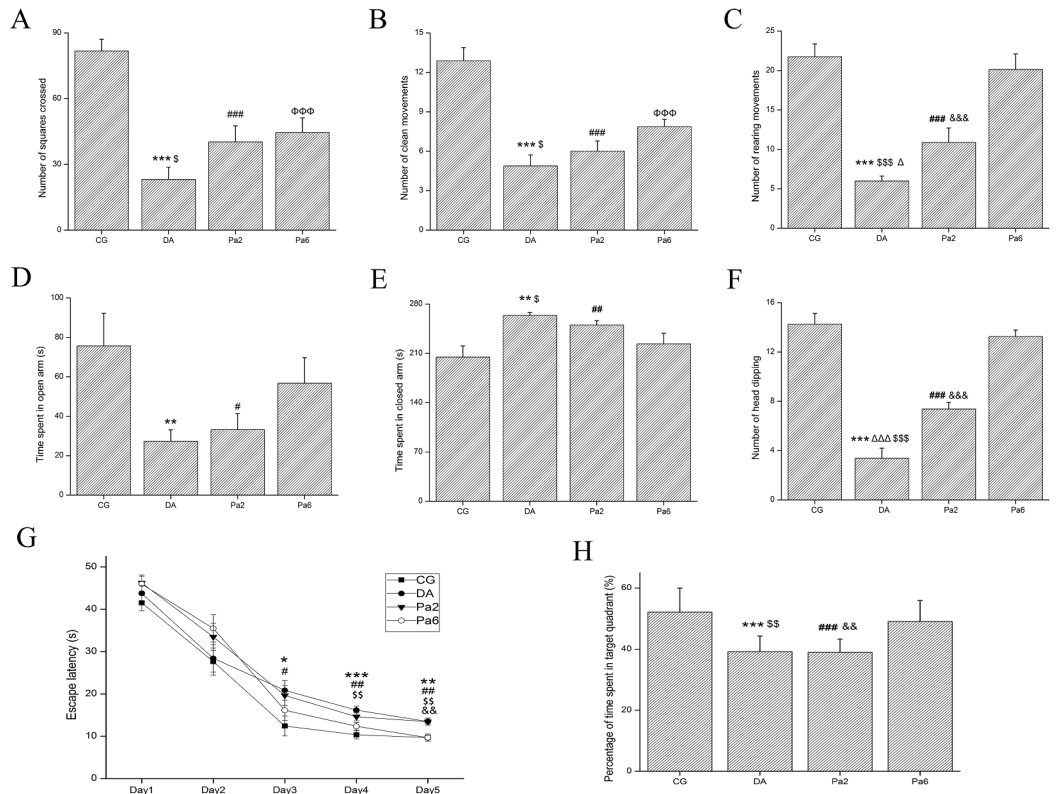


Fig 1. Effects of Pa on the behavioral performances in the OFT (A-C), EPMT (D-F) and MWMT (G, H) ($n = 8-10$). Pa treatment (50 mg/kg, i.p.) attenuated the $D\text{-gal}$ and AlCl_3 -induced decrease in the number of squares crossed (A), the number of clean movements (B), and the number of rears (C) in the OFT. In the EPMT, $D\text{-gal}$ and AlCl_3 induced a decrease in the time spent in open arms (D), which was not significantly improved by Pa treatment. However, Pa attenuated the decrease in the number of head dipping (F) and alleviated the increase in the time spent in closed arms (E). (G) The average escape latencies of four acquisition trials per day in DA rats from days 3 to 5 were significantly more than those in CG rats. Pa pretreatment for 6 weeks produced significant protective effects, particularly at days 4–5. (H) Probe trials 24 h after acquisition trials indicated that animals in Pa6 pre-treated with Pa for 6 weeks spent more time in the target quadrant than animals in DA. Data expressed as the means \pm SEM. * $P < 0.05$, ** $P < 0.01$, *** $P < 0.001$, DA versus CG; # $P < 0.05$, ## $P < 0.01$, ### $P < 0.001$, Pa2 versus CG; ΦΦΦ $P < 0.001$, Pa6 versus CG; Δ $P < 0.05$, ΔΔΔ $P < 0.001$, DA versus Pa2; \$ $P < 0.05$, \$\$ $P < 0.01$, \$\$\$ $P < 0.001$, DA versus Pa6; & $&P < 0.01$, && $&P < 0.001$, Pa2 versus Pa6.

<https://doi.org/10.1371/journal.pone.0185102.g001>

As shown in Fig 1D–1F, there were significant effects of group on the time spent in the open arms ($P < 0.05$), the time spent in the closed arms ($P < 0.01$) and the number of head dipping ($P < 0.001$) in the EPMT. Compared with DA, the rats in Pa6 showed a significant decrease in the time spent in the closed arms ($P < 0.05$) and a significant increase in the number of head dipping ($P < 0.001$).

In the MWMT, the average escape latencies of the four trials per day of each group are detailed in Fig 1G. A repeated ANOVA indicated significant effects of both factors (days: $F_{3,36} = 795.499$, $P < 0.001$; group: $F_{3,36} = 4.239$, $P < 0.05$) and no significant interaction ($F_{3,36} = 2.584$, $P > 0.05$). On the fifth day, pairwise comparisons showed that significant differences were identified between CG and DA ($P < 0.01$), as well as DA and Pa6 ($P < 0.01$), in contrast to CG and Pa6 ($P > 0.05$) (Fig 1G). The probe trial performances were assessed by removing the platform 24 h after the acquisition trials. Multiple comparisons indicated that the time spent in the target quadrant during the probe trial of the animals was significantly more in Pa6 than DA ($P < 0.01$) (Fig 1H).

To evaluate the curative effects of Pa on *D*-gal and AlCl₃-induced behavioral damage, rats were treated with Pa (50 mg/kg) for 2 weeks following administration with *D*-gal and AlCl₃ for 4 weeks. Treatment with Pa for 2 weeks also increased the sum of rears in the OFT ($P<0.05$) (Fig 1C) and upregulated the number of head dipping in the EPMT ($P<0.001$) (Fig 1F). Our data suggest that Pa can alleviate *D*-gal and AlCl₃-induced decreases in animal locomotor activity, performances of anxiety behaviors, and learning and memory impairments.

Pa alleviated *D*-gal and AlCl₃-induced A β and p-tau burdens in the hippocampus

The remarkable pathological features of AD include excess A β deposits and the formation of hyperphosphorylated-tau. Histological observation indicated that the Pa-pretreated rats had less A β_{1-42} -positive deposits and p-tau positive inclusions than the vehicle-matched controls as visualized by immunostaining (using anti-A β_{1-42} and -p-tau antibodies) (Fig 2A and 2B). One-way ANOVA indicated differences between the groups in the percentage areas of the A β_{1-42} -positive deposits ($P<0.001$) and the number of p-tau positive cells ($P<0.001$) (Fig 2D and 2E). Two-tailed *t* tests indicated that Pa treatment for two weeks and Pa pretreatment for six weeks led to 58.4% ($P<0.001$) and 93.8% ($P<0.001$) reductions of hippocampal A β_{1-42} burdens, respectively, and 35.4% ($P<0.001$) and 66.3% ($P<0.001$) reductions of hyperphosphorylated-tau burdens, respectively.

Western blot bands of the A β oligomers indicated visible differences between the groups (Fig 2C). What type of A β oligomers has neurotoxicity? Many studies have focused on ~56 KD [70], as well as ~32 KD A β oligomers [71–73]. In this study, we analyzed ~16 KD, ~28 KD, ~32 KD and ~56 KD A β oligomers. Pre-treatment with Pa for 6 weeks remarkably reduced the formations of A β oligomers of ~28 KD, ~32 KD and ~56 KD. The administration of Pa for 2 weeks also resulted in a significant reduction of A β oligomers of ~28 and ~56 KD (Fig 2F–2I). Our results indicate that Pa reduces A β deposits, hyperphosphorylated-tau formations, and toxic A β oligomer productions.

Pa reduced dendritic spine loss and dendritic atrophy in the hippocampus

In general, it is accepted that toxic A β oligomers cause synaptic and dendritic spine loss [74–77], which are highly associated with the behavior abnormalities widely observed in several psychiatric disorders and neurodegenerative diseases, such as AD [16, 18, 19]. More than 90% of excitatory synapses are formed on dendritic spines that protrude from the main dendritic shaft (reviewed in Nimchinsky et al. 2002) [78]. Therefore, we evaluated the effects of Pa on *D*-gal and AlCl₃-induced dendritic injury, including the dendritic branch and length and the density and types of dendritic spines, in hippocampal pyramidal and granular cells.

Fig 3A presents the pyramidal neurons of CA1 in CG, DA, Pa2, and Pa6. Sholl analysis indicated that Pa pretreatment for 6 weeks prominently alleviated the *D*-gal and AlCl₃-induced reduction of dendritic length and branching in both pyramidal cells of the CA1 (Fig 3B–3D) and CA3 (Fig 3E–3G) and granular cells of the DG (Fig 3H and 3I). Treatment with Pa for 2 weeks did not significantly affect the length of dendrites or the number of intersections.

As shown in Fig 4A, the slice view of dendritic segments indicated visible differences in the morphology and number of dendritic spines between the groups. In this study, three types of dendritic spines, mushroom / branched (MB, width > 0.6 μ m or “branch”), stubby (ST, length: width ratio (LWR) ≤ 1 and length < 1 μ m), and filopodia / thin (FT, length > 1 μ m or LWR > 1), were automatically divided by reconstruct software by analyzing the Z-stacks. Pre-treatment of Pa for 6 weeks significantly alleviated the *D*-gal and AlCl₃-induced decrease in

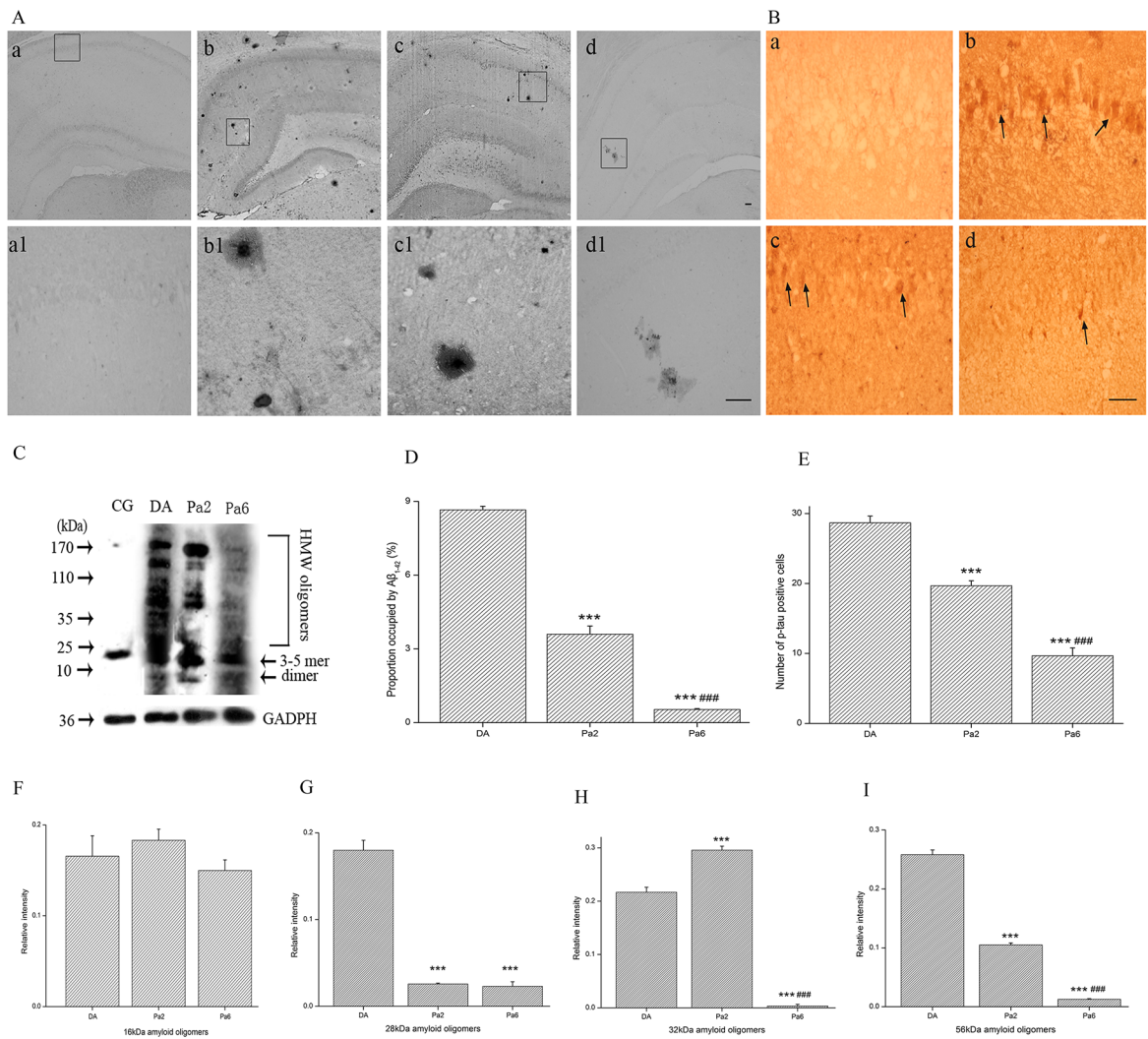


Fig 2. Pa alleviated *D*-gal and AlCl_3 -induced $\text{A}\beta$ and tau burdens in the hippocampus. (A) Grayscale microscope pictures in immunohistochemical staining with $\text{A}\beta_{42}$ antibody in the hippocampus in CG (a), DA (b), Pa2 (c), and Pa6 (d) and their magnifications (a', b', c', and d', respectively). (B) Phospho-tau immunohistochemical staining (p-Ser 202) in the hippocampus in CG (a), DA (b), Pa2 (c), and Pa6 (d). (C) Western blot bands with A11 antibody identifying different molecular weights of $\text{A}\beta$ oligomers in the hippocampus in CG (left column), DA (middle left column), Pa2 (middle right column), and Pa6 (right column). Administration of Pa (50 mg/kg, i.p.) for 2 or 6 weeks significantly reduced the percentage area of $\text{A}\beta_{42}$ -positive deposits (D) and the number of p-tau positive cells (E). Pa did not affect the expression of 16 KD $\text{A}\beta$ oligomers (F); however, it decreased the expression of 28 KD $\text{A}\beta$ oligomers after the treatment of Pa for 2 or 6 weeks (G), downregulated the expression of 36 KD $\text{A}\beta$ oligomers after the treatment of Pa for 6 weeks (H), and reduced the expression of 56 KD $\text{A}\beta$ oligomers after the treatment of Pa for 2 or 6 weeks (I). Data expressed as the means \pm SEM ($n = 4\sim 5$). *** $P < 0.001$, versus DA; # $P < 0.001$, versus Pa2. Scales: 100 μm in A (d1) and 50 μm in B (d).

<https://doi.org/10.1371/journal.pone.0185102.g002>

the spine density of the CA1 apical proximal dendrites and basal dendrites (Fig 4B), CA3 apical proximal dendrites (Fig 4F), and DG apical proximal and distal dendrites (Fig 4J). Pa pre-treatment for 6 weeks substantially increased the percentage of MB spines in the CA1 apical distal dendrites (Fig 4D), CA3 basal dendrites (Fig 4I), and DG apical proximal dendrites (Fig 4K), upregulated the percentage of ST spines in the DG apical distal dendrites (Fig 4L), and reduced the percentage of FT spines in the CA1 basal dendrites (Fig 4E), as well as in the DG apical proximal (Fig 4K) and distal dendrites (Fig 4L). Treatment with Pa for 2 weeks also significantly alleviated the *D*-gal and AlCl_3 -induced decrease in the spine density of the CA3

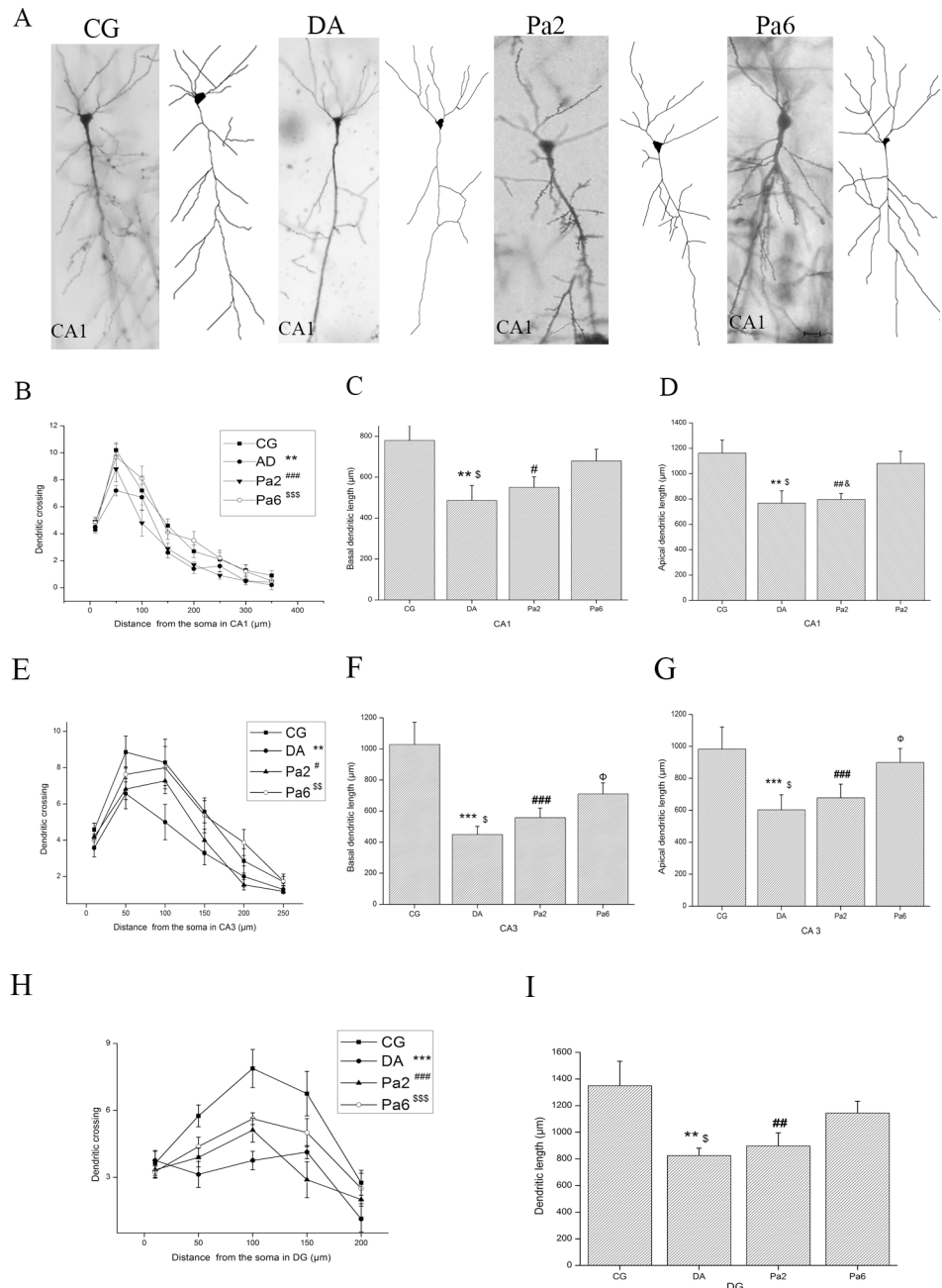
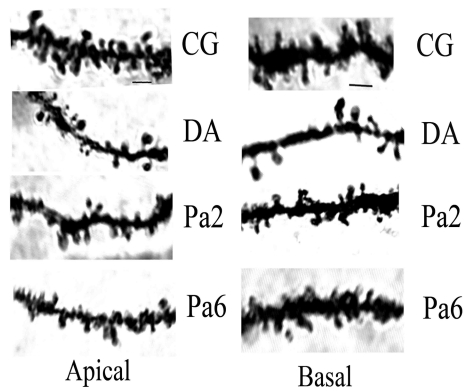


Fig 3. Pa attenuated the decrease in dendritic length and branches in hippocampal CA1 (B-D), CA3 (E-G) and DG (H-I). (A) CA1 pyramidal neurons and their traces drawn by ImageJ software. Pa pretreatment (50 mg/kg, i.p.) for 6 weeks significantly increased the number of dendritic branches in CA1 (B), CA3 (E), and DG (H), extended the length of basal dendrites in CA1 (C) and CA3 (F), and increased the length of apical dendrites in CA1 (D), CA3 (G), and DG (I). However, Pa treatment for 2 weeks did not significantly affect the dendritic branch or length in hippocampal neurons. Data expressed as the means \pm SEM ($n = 8\sim 10$). ** $P < 0.01$, *** $P < 0.001$, DA versus CG; # $P < 0.05$, ## $P < 0.01$, ### $P < 0.001$, Pa2 versus CG; $\ddagger P < 0.05$, Pa6 versus CG; \$ $P < 0.05$, \$\$P < 0.01, DA versus Pa6; & $P < 0.05$, Pa2 versus Pa6.

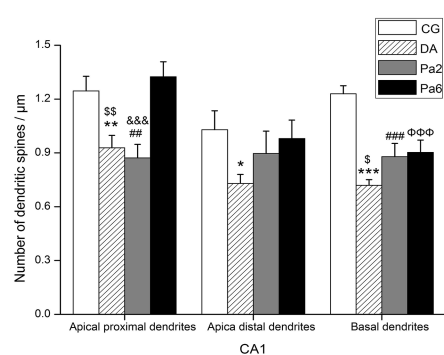
<https://doi.org/10.1371/journal.pone.0185102.g003>

apical proximal dendrites (Fig 4F) and DG apical proximal dendrites (Fig 4I). These data suggest that Pa reduces D -gal and $AlCl_3$ -induced dendritic spine loss, increases the percentage of MB spines, and downregulates the percentage of FT spines in a region-dependent manner.

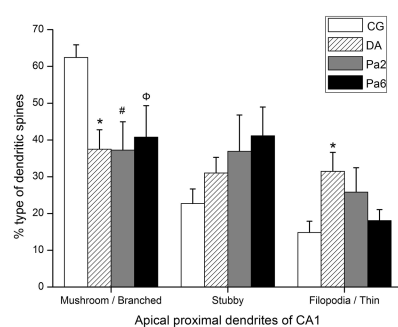
A



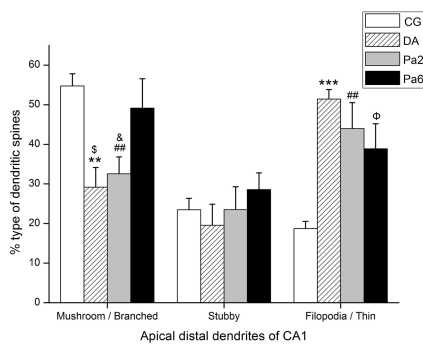
B



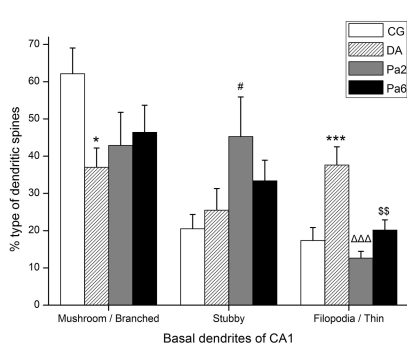
C



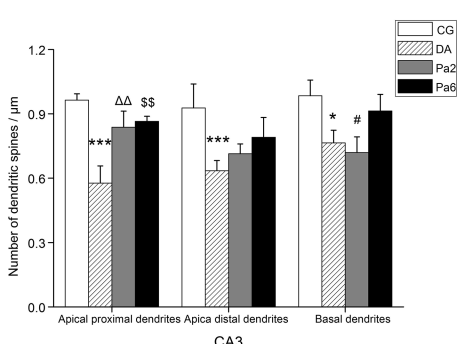
D



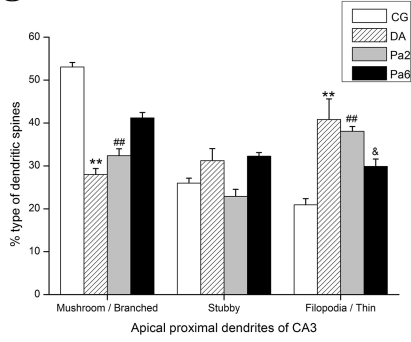
E



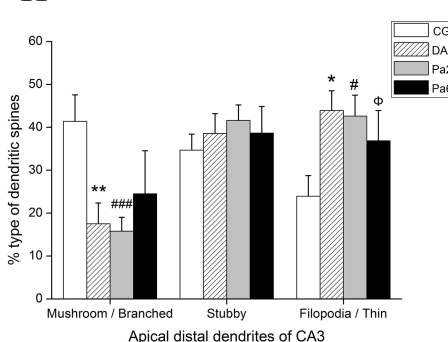
F



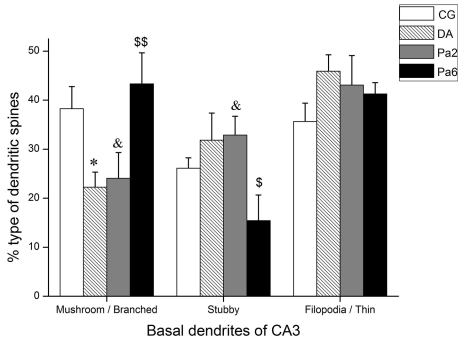
G



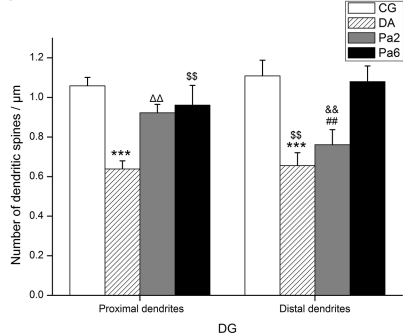
H



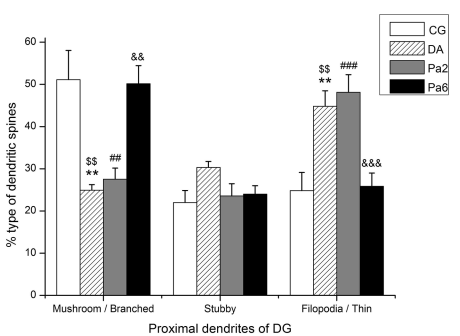
I



J



K



L

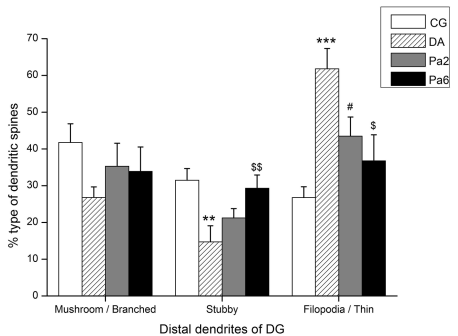


Fig 4. Effects of Pa on density and type of dendritic spines in hippocampal CA1 (B-E), CA3 (F-I) and DG (J-L). (A) Slice view acquired by Laser scanning confocal microscope (FV1000, 60×6 for objective magnification) at the apical proximal (left column) and basal (right column) dendritic segments stained by Golgi-Cox method in CA1 of CG, DA, Pa2, and Pa6. In CA1, Pa pretreatment for 6 weeks significantly increased the dendritic spine density in apical proximal dendrites and basal dendrites but not in apical distal dendrites (B), reduced the percentage of filopodia / thin in basal dendrites (C), and increased the percentage of mushroom / branched in apical distal dendrites (E); however, it did not significantly affect the percentage of various types of dendritic spines in apical proximal dendrites (D). Treatment with Pa for 2 weeks only reduced the percentage of filopodia / thin in basal dendrites. In CA3, pretreatment of Pa for 6 weeks increased the dendritic spine density in apical proximal dendrites (F), reduced the percentage of filopodia / thin in apical proximal dendrites (G), upregulated the percentage of mushroom / branched in basal dendrites (I), and downregulated the percentage of stubby in basal dendrites (I); however, it did not significantly affect the percentage of various types of dendritic spines in apical distal dendrites (H). Treatment of Pa for 2 weeks also increased the dendritic spine density in apical proximal dendrites (F). In the DG, the dendritic spine density of apical proximal and distal dendrites was higher in Pa-treated groups than vehicle-matched controls (J). The percentage of mushroom / branched was increased and the percentage of filopodia / thin was reduced in apical proximal dendrites after 6 weeks pretreatment with Pa (K), whereas the percentage of stubby was increased and the percentage of filopodia / thin was reduced in apical distal dendrites after 6 weeks pretreatment of Pa (L). Data expressed as the means ± SEM ($n = 8\text{--}10$). * $P < 0.05$, ** $P < 0.01$, *** $P < 0.001$, DA versus CG; # $P < 0.05$, ## $P < 0.01$, Pa2 versus CG; ^ $P < 0.05$, ^ΦΦΦ $P < 0.001$, Pa6 versus CG; △△ $P < 0.01$, △△△ $P < 0.001$, DA versus Pa2; \$ $P < 0.05$, \$\$ $P < 0.01$, DA versus Pa6; & $P < 0.05$, && $P < 0.01$, Pa2 versus Pa6.

<https://doi.org/10.1371/journal.pone.0185102.g004>

Pa alleviated *D*-gal and AlCl₃-induced abnormalities of actin remodeling

The dendritic spine cytoskeleton is mainly composed of actin filaments at ~200 nm diameter [79]. Actin remodeling through actin filament nonequilibrium assembly and disassembly governs most, if not all, dendritic spine physiology [80]. Using phalloidin staining, we evaluated the F-actin density and determined that *D*-gal and AlCl₃ induced reductions in F-actin in all statistical regions (Fig 5). Pa pretreatment for 6 weeks alleviated the decrease of F-actin in the apical distal dendritic region and the basal dendritic region of CA1 (Fig 5D), the apical distal dendritic region of CA3 (Fig 5E) and the apical distal dendritic region of DG (Fig 5F), whereas Pa treatment 2 weeks only alleviated the reduction of F-actin in the apical distal dendritic region and the basal dendritic region of CA1 (Fig 5D). The changes in F-actin in different regions of the hippocampus were similar to the alterations in the density of dendritic spines, which indicate that Pa alleviates *D*-gal and AlCl₃-induced abnormalities of actin remodeling.

Pa reduced p-cofilin1/cofilin1 ratio and relieved *D*-gal AlCl₃-induced cofilin1 redistribution and rod-like formation

One of the best known regulators of actin remodeling is cofilin (mainly cofilin1) [81, 82], which may be inactivated by phosphorylation on Ser3 [83, 84] or release from membrane proteins [75]. Moderately activated cofilin is required for actin remodeling and synaptic plasticity; however, local excess activated cofilin may form actin-cofilin rods, which, in turn, lead to dendritic spine loss and dendrite atrophy [81, 85]. Aβ_{1–42} induces the formation of rods via activation (dephosphorylation) of cofilin in cultured hippocampal neurons [86]. Forebrain-specific deletion of cofilin leads to impairment of all types of associative learning [87]. Therefore, we investigated cofilin1 expression and distribution in the hippocampus. In this study, Western blot analysis showed that the p-cofilin1 (Ser 3) levels were significantly different between the groups ($P < 0.01$), whereas the cofilin1 levels were not different between the groups ($P > 0.05$); however, the administration of Pa for 6 or 2 weeks significantly lowered the p-cofilin1 levels and p-cofilin1/ cofilin1 ratio (p-cofilin1 levels: DA vs Pa6, $P < 0.01$; p-cofilin1/ cofilin1 ratio: DA vs Pa2, $P < 0.01$; DA vs Pa6, $P < 0.001$) (Fig 6N–6Q).

Immunofluorescence technique indicated that cofilin1 immunoreactivity was predominantly distributed in the cytoplasm- and nucleus- perimembranes and processes particularly in the cells morphologically similar to the neural stem cells (NSCs) in the subgranular zone (SGZ) of the dentate gyrus in the CG group (Fig 6A and 6E). *D*-gal and AlCl₃ induced an increased distribution of cofilin1 in the cytoplasm (Fig 6I). Rod-like inclusions may be observed in neuronal processes (Fig 6M). Immunopositive p-cofilin1 primarily distributed in nuclei in the CG (Fig 6B and 6F), and *D*-gal and AlCl₃ promoted the distribution of p-cofilin1

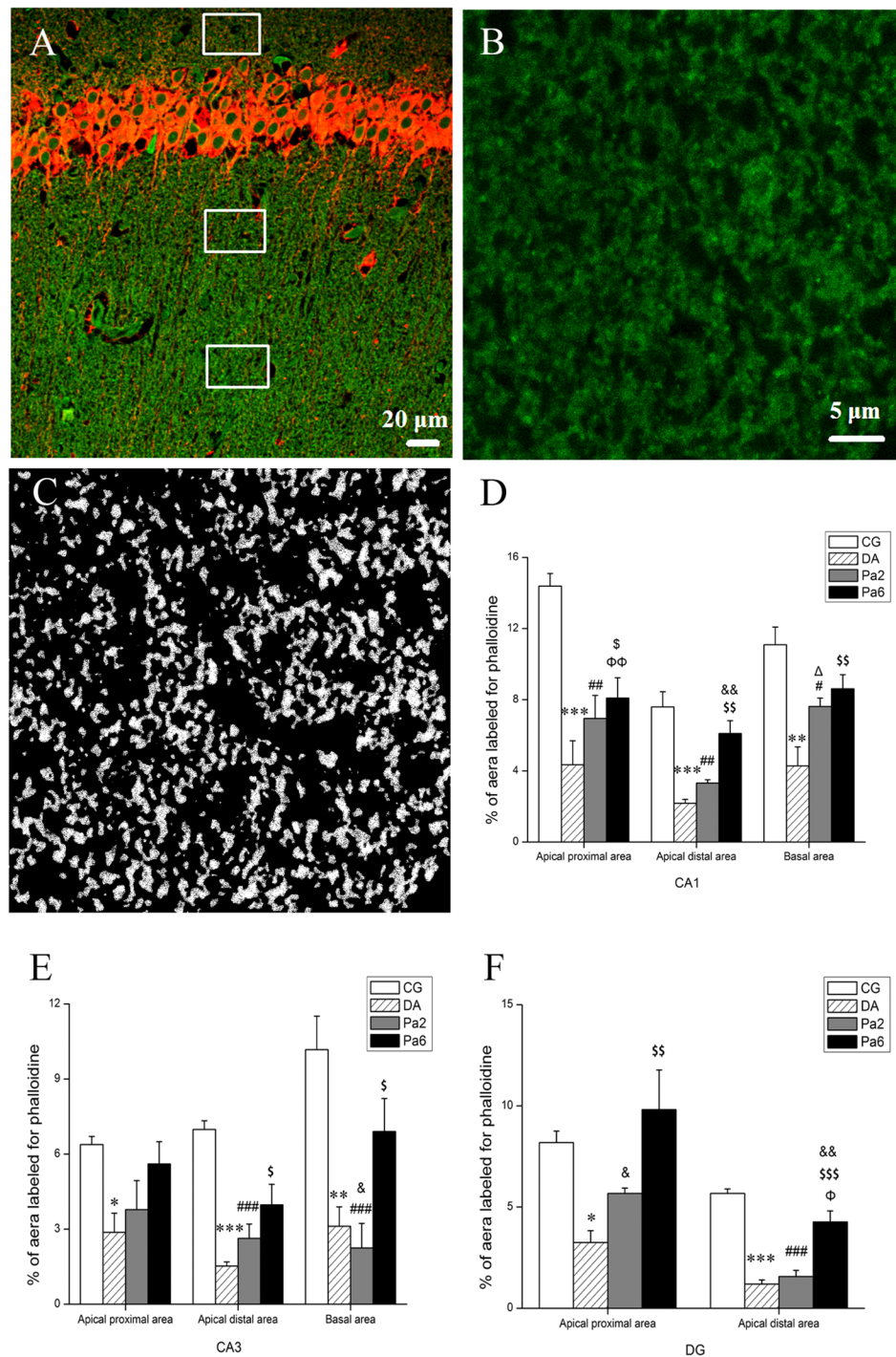


Fig 5. Effects of Pa on F-actin density assessed by phalloidin staining in different areas of hippocampus were analyzed with ImageJ. (A) A schematic diagram of the statistics area in the hippocampus. MAP2 immunoreactivity (red) was used to distinguish the different areas of the hippocampus. (B) Magnification of the statistics area in a single channel of 488 nm (OLYMPUS FV1000). (C) Image of (B) was processed using ImageJ software. The background was subtracted with a rolling value of 15, converted to 8-bit deep images and binarized using a determined threshold value (reduce noise 5, particles 2 - ~). The percentage of phalloidin immunopositive area in apical proximal and distal area and basal area in the hippocampal CA1 (D) and CA3 (E). (F) The percentage of phalloidin immunopositive area in apical proximal and distal area of DG. Data expressed as the means \pm SEM ($n = 3\text{--}5$). Scale bar in (A) represents 20 μm and in (B) represents 5 μm. * $P < 0.05$, ** $P < 0.01$, *** $P < 0.001$, DA versus CG; # $P < 0.05$, ## $P < 0.01$, Pa2 versus CG; Φ $P < 0.05$, $\Phi\Phi$ $P < 0.01$, Pa6 versus

CG; $\Delta P < 0.05$, DA versus Pa2; $\$ P < 0.05$, $\$$ P < 0.01$, $\$\$ P < 0.001$, DA versus Pa6; $\& P < 0.05$, $\&\& P < 0.01$, Pa2 versus Pa6.

<https://doi.org/10.1371/journal.pone.0185102.g005>

in the cytoplasm (**Fig 6J**). Pa pretreatment for six weeks relieved *D*-gal and AlCl₃-induced cofilin1/p-cofilin1 redistribution and attenuated the rod-like formation. Co-immunoreactivity of cofilin1 and p-cofilin1 was detected in some nuclei or processes both in the CG and DA groups. These findings suggest that both cofilin1 activation by release from the membrane and cofilin1 inactivation by phosphorylation on Ser 3 may be involved in actin remodeling and neuronal damage processes.

Pa downregulated RAC1/CDC42 expression in the hippocampus

Small GTPases of the Rho family, such as RAC1/CDC42, mediate the effects of Aβ on actin cytoskeleton dynamics by affecting cofilin activity [88, 89]. Therefore, we further examined the effects of Pa on small GTPases of the RHO family, including RAC1, CDC42 and RHOA.

Western blot analysis showed that the combined induction of *D*-gal and AlCl₃ increased the expressions of RAC1 (**Fig 7B**), CDC42 (**Fig 7C**), and RHOA (**Fig 7D**). Pre-treatment with Pa for 6 weeks did not induce a significant reduction of RHOA (DA vs Pa6, $P > 0.05$); however, it decreased RAC1 (DA vs Pa6, $P < 0.01$) and CDC42 (DA vs Pa6, $P < 0.001$) expression. Treatment with Pa for 2 weeks also significantly decreased RAC1 (DA vs Pa2, $P < 0.05$) and CDC42 (DA vs Pa2, $P < 0.05$) expression, which suggests that the effects of Pa on *D*-gal and AlCl₃-induced disturbance in actin cytoskeleton dynamics may be mediated by RAC1/CDC42.

Discussion

In AD patients, the major causes of cognitive impairments are considered to be neurite atrophy and synaptic loss, which are caused by toxic Aβ, particularly Aβ oligomers [70, 90–92]. In this study, the novelty of our work was to show that Pa alleviated *D*-gal and AlCl₃-induced behavior damages as evaluated by the OFT (**Fig 1A–1C**), EPM (**Fig 1D–1F**), and MWM (**Fig 1G and 1H**). These behavioral disorders may be caused by *D*-gal and AlCl₃-induced excessive productions of Aβ oligomers at ~28, ~36, and ~56 KDs (**Fig 2G–2I**) because these Aβ oligomers, particularly the ~56KD Aβ oligomer [13, 14, 70], highly correlate with impaired behaviors [93]. Consistent alterations with the Aβ oligomer changes included the dendritic spine density (**Fig 4**) and dendritic length and branching in our study (**Fig 3**). The alterations of dendritic spines highly concurred with the dynamics of the actin skeleton, accompanied by the disturbance of cofilin1 activity and the corresponding changes in RAC1/CDC42. These data suggest that Pa can deter formations of detrimental Aβ via the RAC1/CDC42 pathway, cause the redistribution of cofilin1 and decrease of the p-cofilin1/cofilin1 ratio (**Fig 6**), reduce rod-like formation (**Fig 6**) and synaptic and dendritic loss (**Figs 3 and 4**), and ultimately improve the behavioral defects.

Different forms of Aβ, including fibrillar amyloid β (fAβ) [94, 95] and soluble Aβ oligomers (sAβ) [19, 75, 96], have been reported as key players involved in AD pathogenesis [97]. They may cause dendritic spine loss and dendrite atrophy [17, 19, 98]. In rat hippocampal slices, acute overproduction of axonal or dendritic Aβ from APP/tomato-expressing viral-infected neurons reduces the spine density and plasticity at nearby dendrites [77]. Spine loss in number and shift of shape from mushroom to stubby are also observed in organotypic hippocampal slice cultures from Aβ of amyloid precursor protein transgenic mice [99]. Both in over-expressed human APP animal models and AD patients, a significant reduction in the number of dendritic spines and changes in dendritic morphology have been reported [17]. The present

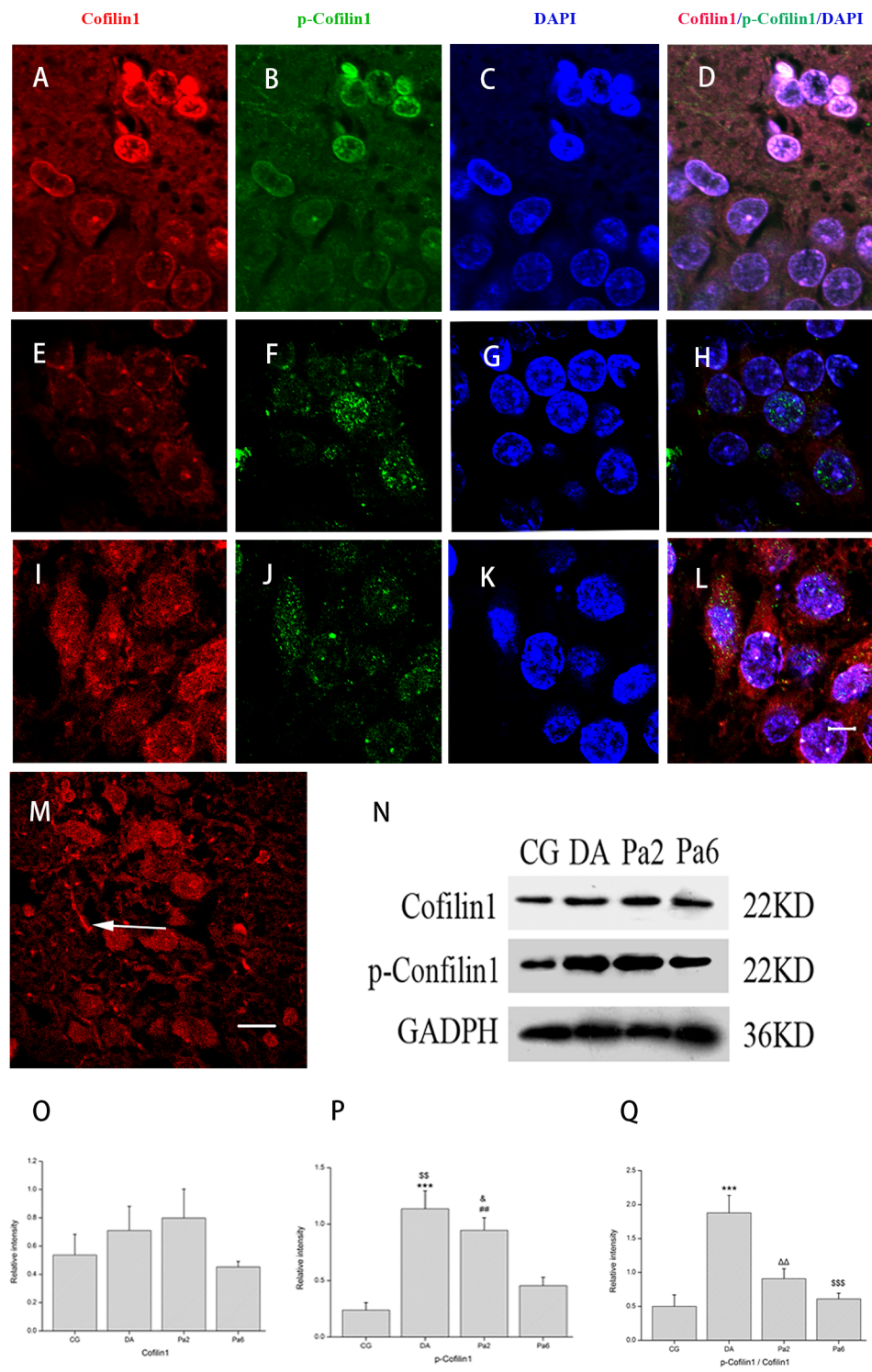


Fig 6. Effects of Pa on cofilin1- and p-cofilin1-immunoreactivity and their hippocampal levels.
 Immunofluorescence labels of cofilin1 (red, excitation wavelength 543/emission wavelength bp560-615), p-cofilin1 (green, excitation wavelength 488/emission wavelength bp500-530) and nucleus (blue, excitation wavelength 458/emission wavelength bp400-461) in DG of CG (A-H) and CA1 of DA (I-M). (N) Western blot for cofilin1 (sc-53934, USA) and p-cofilin1 on Ser 3 (bs-20261R, China) in CG, DA, Pa2, and Pa6. Pa downregulated the p-cofilin1 expression (C) and p-cofilin1/cofilin1 ratio (D); however, it did not affect the cofilin1 level (B). Arrows indicate rod-like inclusions. Data expressed as the means \pm SEM ($n = 3\sim 5$).

*** $P<0.001$, DA versus CG; ** $P<0.01$, Pa2 versus CG; $\Delta\Delta P<0.01$, DA versus Pa2; \$\$P<0.01, \$\$\$P<0.001, DA versus Pa6; & $P<0.05$ Pa2 versus Pa6. Scale bar represents 20 μ m.

<https://doi.org/10.1371/journal.pone.0185102.g006>

evidence by Golgi staining and three-dimensional reconstruction of the series of pictures also showed that with the increase of A β oligomers, significant decreases in the dendritic length and spine density were detected in the DA group, consistent with the previously described studies.

Pa treatment (50 mg/kg, i.p.) consistently increased the dendritic length and branching and the dendritic spine density in all assessed regions of the hippocampus (**Figs 3, 4B, 4F and 4H**); however, the effects of Pa on the proportion of different types of dendritic spines in different regions were different (**Fig 4C, 4E, 4G, 4I and 4J**), which suggests a selective role of Pa is mainly to attenuate the loss of mushroom/branched spines, the main postsynaptic type of functional mature spines.

Previous studies have indicated that the spine density of cultured hippocampal neurons is approximately 0.6/ μ m, the largest proportion of which is the stubby type spines, approximately 70% [100, 101]. However, electron microscopy studies have shown that the largest proportion of hippocampal CA1 spines in adult rats is the thin type spines, approximately 60% [102]. In this study, the spine density was approximately 1.2/ μ m, and the largest proportion was the mushroom / branched spines, approximately 50%, in the CG group (**Fig 4**). Morphological changes of dendritic spines, such as spine maturation, newborn, shrinkage, and devastation, are mainly dependent on the remodeling of the cytoskeleton protein actin [103–105], which is

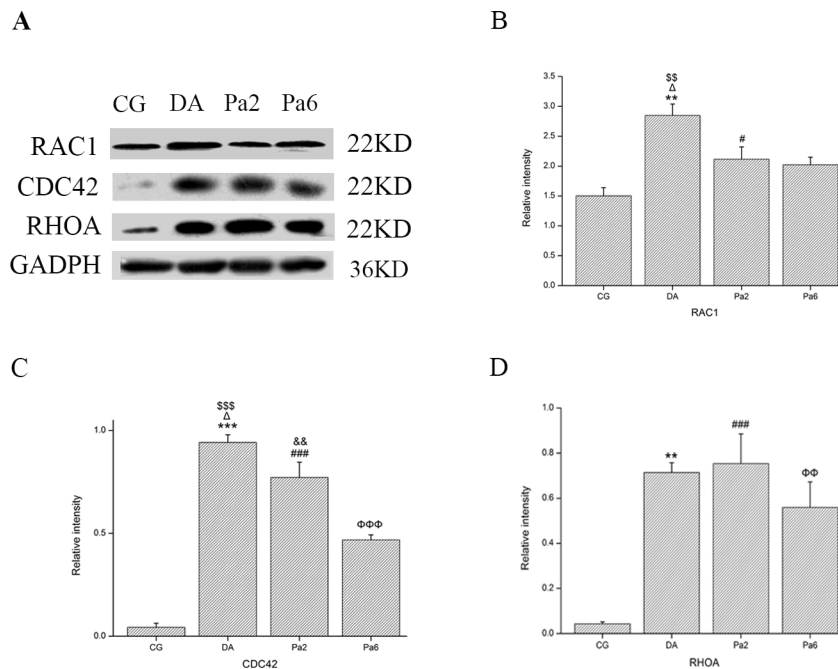


Fig 7. Effects of Pa on RAC1, CDC42 and RHOA. (A) Western blot bands of the hippocampal tissues determined with RAC1, CDC42, and RHOA antibodies in CG (left column), DA (middle left column), Pa2 (middle right column), and Pa6 (right column). GADPH (36KD) is an internal reference. Pre-treatments with Pa (50 mg/kg, i.p.) for 6 weeks significantly alleviated *D*-gal and AlCl₃-induced upregulation of RAC1 (B) and CDC42 (C); however, it did not significantly reduce the expression of RHOA (D). Treatment with Pa for 2 weeks also significantly alleviated *D*-gal and AlCl₃-induced increase of CDC42. Data expressed as the means \pm SEM (n = 3~5). ** $P<0.01$, *** $P<0.001$, DA versus CG; # $P<0.05$, ## $P<0.001$, Pa2 versus CG; ΦΦ $P<0.01$, ΦΦΦ $P<0.001$, Pa6 versus CG; $\Delta\Delta P<0.01$, DA versus Pa2; \$\$P<0.01, \$\$\$P<0.001, DA versus Pa6; && $P<0.01$, Pa2 versus Pa6.

<https://doi.org/10.1371/journal.pone.0185102.g007>

spatiotemporally regulated by numerous actin-binding proteins and upstream signaling molecules [106]. In mammal neurons, cofilin1, an actin-depolymerizing factor (ADF)/cofilin family protein, is widely considered to play an essential role in actin filament dynamics and reorganization [107]. Cofilin1 may be activated by the release of cofilin1 from PtdIns (4, 5) P2 or cortactin or the dephosphorylation of cofilin1 on Ser3 [75]. However, whether an excessive activation [28, 86, 108–111] or inactivation [87, 95, 112–116] of cofilin1 affects the actin-dependent synaptic plasticity and changes the spine shape remains quite controversial [117].

Our results showed that *D*-gal and AlCl₃ did not affect the cofilin1 level; however, they promoted the release of cofilin1 from the plasma membrane into the cytoplasm and increased the formation of rods, which *in vitro* may be induced by excessive levels of active cofilin [109]; these factors were reversed by Pa pretreatment, which suggests that the excessive activation of cofilin1 may be only local particularly in some neuronal processes where rod-like inclusions can block intracellular transport and induce synaptic loss [116]. Different cell types have their own distinct mechanisms of cofilin regulation, and different compartments in one cell have uncoupled regulatory events of cofilin activity [75]. High-resolution imaging has indicated that increased levels of cofilin phosphorylation are a result of cofilin activation by dephosphorylation-independent mechanisms [118]. *D*-gal and AlCl₃ upregulate the p-cofilin1 level and p-cofilin1/cofilin1 ratio and increase cytoplasmic distribution, which is consistent with the proposition that cofilin phosphorylation is involved in recycling cofilin back to the initial starting point in its activity cycle and spatially restricting cofilin activity [119–121]. Therefore, cofilin1 activation and inactivation may both be involved in actin-dependent synaptic plasticity, and Pa attenuation of the *D*-gal and AlCl₃ induced-cofilin1 activation/inactivation is a dynamic spatio-temporal process, not a constant result [98].

It is well-established that extracellular signals, such as Aβ, regulate actin dynamics through the Rho GTPase family. Numerous studies have shown that Rho GTPase family members, RAC1 and RHOA, along with CDC42, work in a coordinated fashion to regulate cell functions, including the regulation of the actin cytoskeleton, cell polarity and migration, gene expression, and cell proliferation [122–126]. Rho GTPases, as molecular switches, bind downstream signals and initiate multiple signaling pathways [127]. Our results that Pa attenuated *D*-gal and AlCl₃-induced upregulation of RAC1/CDC42 suggest that these molecules may be involved in Pa affecting the disturbance of Aβ on actin dynamics and support the hypothesis that cofilin-rod formation disrupts microtubule integrity, blocks intracellular transport, and induces synaptic loss and dendritic atrophy [128].

Supporting information

S1 Fig. Measurement and classification steps for dendritic spines.
(DOC)

Author Contributions

Conceptualization: Fei Han, Ya-Ping Lu.

Data curation: Fei Han, Ting-Ting Zhuang, Jing-Jing Chen, Xiu-Ling Zhu.

Formal analysis: Fei Han.

Methodology: Fei Han, Ting-Ting Zhuang.

Project administration: Fei Han, Xiu-Ling Zhu, Ya-Ping Lu.

Resources: Ya-Ping Lu.

Visualization: Fei Han.

Writing – original draft: Fei Han, Ya-Ping Lu.

Writing – review & editing: Ya-Fei Cai, Ya-Ping Lu.

References

1. Craig L.A., Hong N.S., and McDonald R.J. Revisiting the cholinergic hypothesis in the development of Alzheimer's disease. *Neurosci Biobehav Rev*, 2011; 35(6): 1397–409. <https://doi.org/10.1016/j.neubiorev.2011.03.001> PMID: 21392524.
2. Sarazin M, Berr C, De Rotrou J, Fabrigoule C, Pasquier F, Legrain S, et al. Amnestic syndrome of the medial temporal type identifies prodromal AD: a longitudinal study. *Neurology*, 2007; 69(19):1859–67. <https://doi.org/10.1212/01.wnl.0000279336.36610.f7> PMID: 17984454
3. Blennow K., de Leon M.J., and Zetterberg H. Alzheimer's disease. *The Lancet*, 2006; 368(9533):387–403. [https://doi.org/10.1016/s0140-6736\(06\)69113-7](https://doi.org/10.1016/s0140-6736(06)69113-7) PMID: 16876668
4. Prince M, Bryce R, Albanese E, Wimo A, Ribeiro W, Ferri CP. The global prevalence of dementia: a systematic review and metaanalysis. *Alzheimers Dement*, 2013; 9(1):63–75 e2. <https://doi.org/10.1016/j.jalz.2012.11.007> PMID: 23305823
5. Scheltens P, Blennow K, Breteler MM, de Strooper B, Frisoni GB, Salloway S, et al. Alzheimer's disease. *Lancet*, 2016; 388(10043):505–17. [https://doi.org/10.1016/S0140-6736\(15\)01124-1](https://doi.org/10.1016/S0140-6736(15)01124-1) PMID: 26921134
6. Karvan E., Mercken M., and De Strooper B. The amyloid cascade hypothesis for Alzheimer's disease: an appraisal for the development of therapeutics. *Nat Rev Drug Discov*, 2011; 10(9): 698–712. <https://doi.org/10.1038/nrd3505> PMID: 21852788
7. Ashe K.H. and Zahs K.R. Probing the biology of Alzheimer's disease in mice. *Neuron*, 2010; 66(5):631–45. <https://doi.org/10.1016/j.neuron.2010.04.031> PMID: 20547123
8. Bertram L., Lill C.M., and Tanzi R.E. The genetics of Alzheimer disease: back to the future. *Neuron*, 2010; 68(2):270–81. <https://doi.org/10.1016/j.neuron.2010.10.013> PMID: 20955934
9. Hardy J. Has the amyloid cascade hypothesis for Alzheimer's disease been proved? *Curr Alzheimer Res*, 2006; 3(1):71–3. PMID: 16472206
10. Musiek E.S. and Holtzman D.M. Three dimensions of the amyloid hypothesis: time, space and 'wing-men'. *Nat Neurosci*, 2015; 18(6): 800–6. <https://doi.org/10.1038/nn.4018> PMID: 26007213
11. Herrup K. The case for rejecting the amyloid cascade hypothesis. *Nat Neurosci*, 2015; 18(6): 794–9. <https://doi.org/10.1038/nn.4017> PMID: 26007212
12. De Strooper B. Proteases and proteolysis in Alzheimer disease: a multifactorial view on the disease process. *Physiol Rev*, 2010; 90(2):465–94. <https://doi.org/10.1152/physrev.00023.2009> PMID: 20393191
13. Gong Y, Chang L, Viola KL, Lacor PN, Lambert MP, Finch CE, et al. Alzheimer's disease-affected brain: presence of oligomeric A beta ligands (ADDLs) suggests a molecular basis for reversible memory loss. *Proc Natl Acad Sci U S A*, 2003; 100(18):10417–22. <https://doi.org/10.1073/pnas.1834302100> PMID: 12925731
14. Klein W.L., Stine W.B. Jr., and Teplow D.B.. Small assemblies of unmodified amyloid beta-protein are the proximate neurotoxin in Alzheimer's disease. *Neurobiol Aging*, 2004; 25(5):569–80. <https://doi.org/10.1016/j.neurobiolaging.2004.02.010> PMID: 15172732
15. Oddo S, Caccamo A, Tran L, Lambert MP, Glabe CG, Klein WL, et al. Temporal profile of amyloid-beta (Abeta) oligomerization in an in vivo model of Alzheimer disease. A link between Abeta and tau pathology. *J Biol Chem*, 2006; 281(3):1599–604. <https://doi.org/10.1074/jbc.M507892200> PMID: 16282321
16. Fiala J.C., Spacek J., and Harris K.M. Dendritic spine pathology: cause or consequence of neurological disorders? *Brain Res Brain Res Rev*, 2002; 39(1):29–54 PMID: 12086707
17. Maiti P, Manna J, Ilavazhagan G, Rossignol J, Dunbar GL. Molecular regulation of dendritic spine dynamics and their potential impact on synaptic plasticity and neurological diseases. *Neurosci Biobehav Rev*, 2015; 59:208–37. <https://doi.org/10.1016/j.neubiorev.2015.09.020> PMID: 26562682
18. Hering H. and Sheng M. Dendritic spines: structure, dynamics and regulation. *Nat Rev Neurosci*, 2001; 2(12):880–8. <https://doi.org/10.1038/35104061> PMID: 11733795
19. Sala C. and Segal M. Dendritic spines: the locus of structural and functional plasticity. *Physiol Rev*, 2014; 94(1):141–88. <https://doi.org/10.1152/physrev.00012.2013> PMID: 24382885

20. Masliah E, Mallory M, Hansen L, Alford M, Albright T, DeTeresa R, et al. Patterns of aberrant sprouting in Alzheimer's disease. *Neuron*, 1991; 6(5): 729–39 PMID: 1827266
21. Terry RD, Masliah E, Salmon DP, Butters N, DeTeresa R, Hill R, et al. Physical basis of cognitive alterations in Alzheimer's disease: synapse loss is the major correlate of cognitive impairment. *Ann Neurol*, 1991; 30(4):572–80. <https://doi.org/10.1002/ana.410300410> PMID: 1789684
22. Serrano-Pozo A, Frosch MP, Masliah E, Hyman BT. Neuropathological alterations in Alzheimer disease. *Cold Spring Harb Perspect Med*, 2011; 1(1):a006189. <https://doi.org/10.1101/cshperspect.a006189> PMID: 22229116
23. Boekhoorn K, Terwel D, Biemans B, Borghgraef P, Wiegert O, Ramakers GJ, et al. Improved long-term potentiation and memory in young tau-P301L transgenic mice before onset of hyperphosphorylation and tauopathy. *J Neurosci*, 2006; 26(13): 3514–23. <https://doi.org/10.1523/JNEUROSCI.5425-05.2006> PMID: 16571759
24. Dickstein DL, Brautigam H, Stockton SD Jr., Schmeidler J, Hof PR. Changes in dendritic complexity and spine morphology in transgenic mice expressing human wild-type tau. *Brain Struct Funct*, 2010; 214(2–3):161–79. <https://doi.org/10.1007/s00429-010-0245-1> PMID: 20213269
25. Eckermann K, Mocanu MM, Khlistunova I, Biernat J, Nissen A, Hofmann A, et al. The beta-propensity of Tau determines aggregation and synaptic loss in inducible mouse models of tauopathy. *J Biol Chem*, 2007; 282(43):31755–65. <https://doi.org/10.1074/jbc.M705282200> PMID: 17716969
26. Benilova I, and De Strooper B. Neuroscience. Promiscuous Alzheimer's amyloid: yet another partner. *Science*, 2013; 341(6152): p. 1354–5. <https://doi.org/10.1126/science.1244166> PMID: 24052299
27. De Felice FG, Velasco PT, Lambert MP, Viola K, Fernandez SJ, Ferreira ST, et al. Abeta oligomers induce neuronal oxidative stress through an N-methyl-D-aspartate receptor-dependent mechanism that is blocked by the Alzheimer drug memantine. *J Biol Chem*, 2007; 282(15):11590–601. <https://doi.org/10.1074/jbc.M607483200> PMID: 17308309
28. Kim S., Violette C.J., and Ziff E.B. Reduction of increased calcineurin activity rescues impaired homeostatic synaptic plasticity in presenilin 1 M146V mutant. *Neurobiol Aging*, 2015; 36(12):3239–46. <https://doi.org/10.1016/j.neurobiolaging.2015.09.007> PMID: 26455952
29. Shankar GM, Bloodgood BL, Townsend M, Walsh DM, Selkoe DJ, Sabatini BL. Natural oligomers of the Alzheimer amyloid-beta protein induce reversible synapse loss by modulating an NMDA-type glutamate receptor-dependent signaling pathway. *J Neurosci*, 2007; 27(11): 2866–75. <https://doi.org/10.1523/JNEUROSCI.4970-06.2007> PMID: 17360908
30. Kim T, Vidal GS, Djuricic M, William CM, Birnbaum ME, Garcia KC, et al. Human LirB2 is a beta-amyloid receptor and its murine homolog PirB regulates synaptic plasticity in an Alzheimer's model. *Science*, 2013; 341(6152):1399–404. <https://doi.org/10.1126/science.1242077> PMID: 24052308
31. Scheltens P, Blennow K, Breteler MMB, de Strooper B, Frisoni GB, Salloway S, et al. Alzheimer's disease. *The Lancet*, 2016; 388(10043):505–517. [https://doi.org/10.1016/s0140-6736\(15\)01124-1](https://doi.org/10.1016/s0140-6736(15)01124-1) PMID: 26921134
32. Du Q, Feng GZ, Shen L, Cui J, Cai JK. Paeonol attenuates airway inflammation and hyperresponsiveness in a murine model of ovalbumin-induced asthma. *Can J Physiol Pharmacol*, 2010; 88(10):1010–6. <https://doi.org/10.1139/y10-077> PMID: 20962901
33. Liu MH, Lin AH, Lee HF, Ko HK, Lee TS, Kou YR. Paeonol attenuates cigarette smoke-induced lung inflammation by inhibiting ROS-sensitive inflammatory signaling. *Mediators Inflamm*, 2014; 651890. <https://doi.org/10.1155/2014/651890> PMID: 25165413
34. Liu MH, Lin AH, Lu SH, Peng RY, Lee TS, Kou YR. Eicosapentaenoic acid attenuates cigarette smoke-induced lung inflammation by inhibiting ROS-sensitive inflammatory signaling. *Front Physiol*, 2014; 5: 440. <https://doi.org/10.3389/fphys.2014.00440> PMID: 25452730
35. Tseng YT, Hsu YY, Shih YT, Lo YC. Paeonol attenuates microglia-mediated inflammation and oxidative stress-induced neurotoxicity in rat primary microglia and cortical neurons. *Shock*, 2012; 37(3):312–8. <https://doi.org/10.1097/SHK.0b013e31823fe939> PMID: 22089194
36. Kubes P. and Mehal W.Z. Sterile inflammation in the liver. *Gastroenterology*, 2012; 143(5): 1158–72. <https://doi.org/10.1053/j.gastro.2012.09.008> PMID: 22982943
37. Schroeter H, Boyd CS, Ahmed R, Spencer JP, Duncan RF, Rice-Evans C, et al. c-Jun N-terminal kinase (JNK)-mediated modulation of brain mitochondria function: new target proteins for JNK signaling in mitochondrion-dependent apoptosis. *Biochem J*, 2003; 372(Pt 2):359–69. <https://doi.org/10.1042/BJ20030201> PMID: 12614194
38. Hsieh CL, Cheng CY, Tsai TH, Lin IH, Liu CH, Chiang SY, et al. Paeonol reduced cerebral infarction involving the superoxide anion and microglia activation in ischemia-reperfusion injured rats. *J Ethnopharmacol*, 2006; 106(2):208–15. <https://doi.org/10.1016/j.jep.2005.12.027> PMID: 16458462

39. Liu J, Feng L, Ma D, Zhang M, Gu J, Wang S, et al. Neuroprotective effect of paeonol on cognition deficits of diabetic encephalopathy in streptozotocin-induced diabetic rat. *Neurosci Lett*, 2013; 549:63–8. <https://doi.org/10.1016/j.neulet.2013.06.002> PMID: 23791853
40. Ding Y, Li Q, Xu Y, Chen Y, Deng Y, Zhi F, et al. Attenuating Oxidative Stress by Paeonol Protected against Acetaminophen-Induced Hepatotoxicity in Mice. *PLoS One*, 2016; 11(5):e0154375. <https://doi.org/10.1371/journal.pone.0154375> PMID: 27144271
41. Li H, Song F, Duan LR, Sheng JJ, Xie YH, Yang Q, et al. Paeonol and danshensu combination attenuates apoptosis in myocardial infarcted rats by inhibiting oxidative stress: Roles of Nrf2/HO-1 and PI3K/Akt pathway. *Sci Rep*, 2016; 6: 23693. <https://doi.org/10.1038/srep23693> PMID: 27021411
42. Zhao Y, Fu B, Zhang X, Zhao T, Chen L, Zhang J, et al. Paeonol pretreatment attenuates cerebral ischemic injury via upregulating expression of pAkt, Nrf2, HO-1 and ameliorating BBB permeability in mice. *Brain Res Bull*, 2014; 109: 61–7. <https://doi.org/10.1016/j.brainresbull.2014.09.008> PMID: 25286445
43. Tao W, Wang H, Su Q, Chen Y, Xue W, Xia B, et al. Paeonol attenuates lipopolysaccharide-induced depressive-like behavior in mice. *Psychiatry Research*, 2016; 238:116–121. <https://doi.org/10.1016/j.psychres.2016.02.033> PMID: 27086220
44. Zhou J, Zhou L, Hou D, Tang J, Sun J, Bondy SC. Paeonol increases levels of cortical cytochrome oxidase and vascular actin and improves behavior in a rat model of Alzheimer's disease. *Brain Research*, 2011; 1388:141–147. <https://doi.org/10.1016/j.brainres.2011.02.064> PMID: 21377451
45. Kayed R, Head E, Sarsoza F, Saing T, Cotman CW, Necula M, et al. Fibril specific, conformation dependent antibodies recognize a generic epitope common to amyloid fibrils and fibrillar oligomers that is absent in prefibrillar oligomers. *Mol Neurodegener*, 2007; 2:18. <https://doi.org/10.1186/1750-1326-2-18> PMID: 17897471
46. Li H, Song J, Zhang J, Wang T, Yan Y, Tao Z, et al. Ginseng Protein Reverses Amyloid Beta Peptide and H2 O2 Cytotoxicity in Neurons, and Ameliorates Cognitive Impairment in AD Rats Induced by a Combination of D-Galactose and AlCl3. *Phytother Res*, 2017; 31(2):284–295. <https://doi.org/10.1002/ptr.5747> PMID: 27981642
47. Li H, Kang T, Qi B, Kong L, Jiao Y, Cao Y, et al. Neuroprotective effects of ginseng protein on PI3K/Akt signaling pathway in the hippocampus of D-galactose/AlCl3 inducing rats model of Alzheimer's disease. *J Ethnopharmacol*, 2016; 179:162–9. <https://doi.org/10.1016/j.jep.2015.12.020> PMID: 26721223
48. Jayant S, Sharma BM, Bansal R, Sharma B. Pharmacological benefits of selective modulation of cannabinoid receptor type 2 (CB2) in experimental Alzheimer's disease. *Pharmacol Biochem Behav*, 2016; 140:39–50. <https://doi.org/10.1016/j.pbb.2015.11.006> PMID: 26577751
49. Zhang Y, Yang X, Jin G, Yang X, Zhang Y. Polysaccharides from Pleurotus ostreatus alleviate cognitive impairment in a rat model of Alzheimer's disease. *Int J Biol Macromol*, 2016; 92:935–941. <https://doi.org/10.1016/j.ijbiomac.2016.08.008> PMID: 27498414
50. Xiao Q, Yu W, Tian Q, Fu X, Wang X, Gu M, et al. Chitinase1 contributed to a potential protection via microglia polarization and Abeta oligomer reduction in D-galactose and aluminum-induced rat model with cognitive impairments. *Neuroscience*, 2017; 355:61–70. <https://doi.org/10.1016/j.neuroscience.2017.04.050> PMID: 28499970
51. Xiao F, Li XG, Zhang XY, Hou JD, Lin LF, Gao Q, et al. Combined administration of D-galactose and aluminium induces Alzheimer-like lesions in brain. *Neurosci Bull*, 2011; 27(3):143–55. <https://doi.org/10.1007/s12264-011-1028-2> PMID: 21614097
52. Luo Y, Niu F, Sun Z, Cao W, Zhang X, Guan D, et al. Altered expression of Abeta metabolism-associated molecules from D-galactose/AlCl₃ induced mouse brain. *Mech Ageing Dev*, 2009; 130(4):248–52. <https://doi.org/10.1016/j.mad.2008.12.005> PMID: 19150622
53. Sun ZZ, Chen ZB, Jiang H, Li LL, Li EG, Xu Y. Alteration of Abeta metabolism-related molecules in predementia induced by AlCl₃ and D-galactose. *Age (Dordr)*, 2009; 31(4):277–84. <https://doi.org/10.1007/s11357-009-9099-y> PMID: 19468866
54. Li Z, Zhao G, Qian S, Yang Z, Chen X, Chen J, et al. Cerebrovascular protection of beta-asarone in Alzheimer's disease rats: a behavioral, cerebral blood flow, biochemical and genic study. *J Ethnopharmacol*, 2012; 144(2): 305–12. <https://doi.org/10.1016/j.jep.2012.09.013> PMID: 22985635
55. Walsh R.N. and Cummins R.A. The Open-Field Test: a critical review. *Psychol Bull*, 1976; 83(3): 482–504. PMID: 17582919
56. Pellow S, Chopin P, File SE, Briley M. Validation of open:closed arm entries in an elevated plus-maze as a measure of anxiety in the rat. *J Neurosci Methods*, 1985; 14(3):149–67. PMID: 2864480
57. Morris R. Developments of a water-maze procedure for studying spatial learning in the rat. *J Neurosci Methods*, 1984; 11(1):47–60. PMID: 6471907

58. Gibb R. and Kolb B. A method for vibratome sectioning of Golgi-Cox stained whole rat brain. *J Neurosci Methods*, 1998; 79(1): 1–4. PMID: 9531453
59. Hu XY, Qin S, Lu YP, Ravid R, Swaab DF, Zhou JN. Decreased estrogen receptor-alpha expression in hippocampal neurons in relation to hyperphosphorylated tau in Alzheimer patients. *Acta Neuropathol*, 2003; 106(3):213–20. <https://doi.org/10.1007/s00401-003-0720-3> PMID: 12819990
60. Lu YP, Zeng M, Hu XY, Xu H, Swaab DF, Ravid R, et al. Estrogen receptor alpha-immunoreactive astrocytes are increased in the hippocampus in Alzheimer's disease. *Exp Neurol*, 2003; 183(2): 482–8. PMID: 14552888
61. Lazcano Z, Solis O, Bringas ME, Limon D, Diaz A, Espinosa B, et al. Unilateral injection of Abeta25–35 in the hippocampus reduces the number of dendritic spines in hyperglycemic rats. *Synapse*, 2014; <https://doi.org/10.1002/syn.21770> PMID: 25049192
62. Mavroudis IA, Fotiou DF, Manani MG, Njaou SN, Frangou D, Costa VG, et al. Dendritic pathology and spinal loss in the visual cortex in Alzheimer's disease: a Golgi study in pathology. *Int J Neurosci*, 2011; 121(7):347–54. <https://doi.org/10.3109/00207454.2011.553753> PMID: 21545306
63. Paxinos G. and Watson C. The rat brain in stereotaxic coordinates (6th edition). 2007; Netherlands: Elsevier Academic Press. 1–451.
64. Bringas ME, Carvajal-Flores FN, Lopez-Ramirez TA, Atzori M, Flores G. Rearrangement of the dendritic morphology in limbic regions and altered exploratory behavior in a rat model of autism spectrum disorder. *Neuroscience*, 2013; 241: 170–87. <https://doi.org/10.1016/j.neuroscience.2013.03.030> PMID: 23535253
65. Flores G, Alquicer G, Silva-Gomez AB, Zaldivar G, Stewart J, Quirion R, et al. Alterations in dendritic morphology of prefrontal cortical and nucleus accumbens neurons in post-pubertal rats after neonatal excitotoxic lesions of the ventral hippocampus. *Neuroscience*, 2005; 133(2): 463–70. <https://doi.org/10.1016/j.neuroscience.2005.02.021> PMID: 15878241
66. Kolb B, Fergie M, Gibb R, Gorny G, Rountree S. Age, experience and the changing brain. *Neurosci Biobehav Rev*, 1998; 22(2): 143–59. PMID: 9579307
67. Martinez-Tellez RI, Hernandez-Torres E, Gamboa C, Flores G. Prenatal stress alters spine density and dendritic length of nucleus accumbens and hippocampus neurons in rat offspring. *Synapse*, 2009; 63(9):794–804. <https://doi.org/10.1002/syn.20664> PMID: 19489049
68. Guirado R, Perez-Rando M, Sanchez-Matarredona D, Castren E, Nacher J. Chronic fluoxetine treatment alters the structure, connectivity and plasticity of cortical interneurons. *Int J Neuropsychopharmacol*, 2014; 17(10):1635–46. <https://doi.org/10.1017/S1461145714000406> PMID: 24786752
69. Sadowski MJ, Pankiewicz J, Scholtzova H, Mehta PD, Prelli F, Quartermain D, et al. Blocking the apolipoprotein E/amyloid-beta interaction as a potential therapeutic approach for Alzheimer's disease. *Proc Natl Acad Sci U S A*, 2006; 103(49):18787–92. <https://doi.org/10.1073/pnas.0604011103> PMID: 17116874
70. Lesne SE, Sherman MA, Grant M, Kuskowski M, Schneider JA, Bennett DA, et al. Brain amyloid-beta oligomers in ageing and Alzheimer's disease. *Brain*, 2013; 136(Pt 5):1383–98. <https://doi.org/10.1093/brain/awt062> PMID: 23576130
71. Goni F, Prelli F, Ji Y, Scholtzova H, Yang J, Sun Y, et al. Immunomodulation targeting abnormal protein conformation reduces pathology in a mouse model of Alzheimer's disease. *PLoS One*, 2010; 5(10): e13391. <https://doi.org/10.1371/journal.pone.0013391> PMID: 20967130
72. Washington PM, Morffy N, Parsadanian M, Zapple DN, Burns MP. Experimental traumatic brain injury induces rapid aggregation and oligomerization of amyloid-beta in an Alzheimer's disease mouse model. *J Neurotrauma*, 2014; 31(1):125–34. <https://doi.org/10.1089/neu.2013.3017> PMID: 24050316
73. Yang J, Ji Y, Mehta P, Bates KA, Sun Y, Wisniewski T. Blocking the apolipoprotein E/amyloid-beta interaction reduces fibrillar vascular amyloid deposition and cerebral microhemorrhages in TgSwDI mice. *J Alzheimers Dis*, 2011; 24(2):269–85. <https://doi.org/10.3233/JAD-2011-101401> PMID: 21239853
74. Hsieh H, Boehm J, Sato C, Iwatsubo T, Tomita T, Sisodia S, et al. AMPAR removal underlies Abeta-induced synaptic depression and dendritic spine loss. *Neuron*, 2006; 52(5):831–843. <https://doi.org/10.1016/j.neuron.2006.10.035> PMID: 17145504
75. Shankar GM, Bloodgood BL, Townsend M, Walsh DM, Selkoe DJ, Sabatini BL. Natural oligomers of the Alzheimer amyloid-beta protein induce reversible synapse loss by modulating an NMDA-type glutamate receptor-dependent signaling pathway. *Journal of Neuroscience the Official Journal of the Society for Neuroscience*, 2007; 27(11):2866. <https://doi.org/10.1523/JNEUROSCI.4970-06.2007> PMID: 17360908
76. Spires TL, Meyer-Luehmann M, Stern EA, McLean PJ, Skoch J, Nguyen PT, et al. Dendritic spine abnormalities in amyloid precursor protein transgenic mice demonstrated by gene transfer and

- intravital multiphoton microscopy. *J Neurosci*, 2005; 25(31): 7278–87. <https://doi.org/10.1523/JNEUROSCI.1879-05.2005> PMID: 16079410
77. Wei W, Nguyen LN, Kessels HW, Hagiwara H, Sisodia S, Malinow R. Amyloid beta from axons and dendrites reduces local spine number and plasticity. *Nat Neurosci*, 2010; 13(2):190–6. <https://doi.org/10.1038/nn.2476> PMID: 20037574
78. Leuner B, Gould E, Gould, Structural plasticity and hippocampal function. *Annu Rev Psychol*, 2010; 61:111–40, C1–3. <https://doi.org/10.1146/annurev.psych.093008.100359> PMID: 19575621
79. Frost NA, Shroff H, Kong H, Betzig E, Blanpied TA. Single-molecule discrimination of discrete perisynaptic and distributed sites of actin filament assembly within dendritic spines. *Neuron*, 2010; 67(1):86–99. <https://doi.org/10.1016/j.neuron.2010.05.026> PMID: 20624594
80. Spence E.F. and Soderling S.H. Actin Out: Regulation of the Synaptic Cytoskeleton. *J Biol Chem*, 2015; 290(48):28613–22. <https://doi.org/10.1074/jbc.R115.655118> PMID: 26453304
81. Bernstein B.W. and Bamburg J.R. ADF/cofilin: a functional node in cell biology. *Trends Cell Biol*, 2010; 20(4):187–95. <https://doi.org/10.1016/j.tcb.2010.01.001> PMID: 20133134
82. Pollard T.D. and Borisy G.G. Cellular motility driven by assembly and disassembly of actin filaments. *Cell*, 2003; 112(4):453–65. PMID: 12600310
83. Yang N, Higuchi O, Ohashi K, Nagata K, Wada A, Kangawa K, et al. Cofilin phosphorylation by LIM-kinase 1 and its role in Rac-mediated actin reorganization. *Nature*, 1998; 393(6687): 809–12. <https://doi.org/10.1038/31735> PMID: 9655398
84. Bravo-Cordero JJ, Magalhaes MA, Eddy RJ, Hodgson L, Condeelis J. Functions of cofilin in cell locomotion and invasion. *Nat Rev Mol Cell Biol*, 2013; 14(7): 405–15. <https://doi.org/10.1038/nrm3609> PMID: 23778968
85. Van Troys M, Huyck L, Leyman S, Dhaese S, Vandekerckhove J, Ampe C. Ins and outs of ADF/cofilin activity and regulation. *Eur J Cell Biol*, 2008; 87(8–9):649–67. <https://doi.org/10.1016/j.ejcb.2008.04.001> PMID: 18499298
86. Maloney MT, Minamide LS, Kinley AW, Boyle JA, Bamburg JR. Beta-secretase-cleaved amyloid precursor protein accumulates at actin inclusions induced in neurons by stress or amyloid beta: a feedforward mechanism for Alzheimer's disease. *J Neurosci*, 2005; 25(49):11313–21. <https://doi.org/10.1523/JNEUROSCI.3711-05.2005> PMID: 16339026
87. Rust MB, Gurniak CB, Renner M, Vara H, Morando L, Gorlich A, et al. Learning, AMPA receptor mobility and synaptic plasticity depend on n-cofilin-mediated actin dynamics. *EMBO J*, 2010; 29(11): p. 1889–902. <https://doi.org/10.1038/emboj.2010.72> PMID: 20407421
88. Davis RC, Maloney MT, Minamide LS, Flynn KC, Stonebraker MA, Bamburg JR. Mapping cofilin-actin rods in stressed hippocampal slices and the role of cdc42 in amyloid-beta-induced rods. *J Alzheimers Dis*, 2009; 18(1):35–50. <https://doi.org/10.3233/JAD-2009-1122> PMID: 19542631
89. Edwards DC, Sanders LC, Bokoch GM, Gill GN. Activation of LIM-kinase by Pak1 couples Rac/Cdc42 GTPase signalling to actin cytoskeletal dynamics. *Nat Cell Biol*, 1999; 1(5):253–9. <https://doi.org/10.1038/12963> PMID: 10559936
90. DeKosky S.T. and Scheff S.W. Synapse loss in frontal cortex biopsies in Alzheimer's disease: correlation with cognitive severity. *Ann Neurol*, 1990; 27(5):457–64. <https://doi.org/10.1002/ana.410270502> PMID: 2360787
91. Einstein G., Buranosky R., and Crain B.J. Dendritic pathology of granule cells in Alzheimer's disease is unrelated to neuritic plaques. *J Neurosci*, 1994; 14(8):5077–88. PMID: 8046469
92. Masliah E, Mallory M, Alford M, DeTeresa R, Hansen LA, McKeel DW Jr., et al. Altered expression of synaptic proteins occurs early during progression of Alzheimer's disease. *Neurology*, 2001; 56(1):127–9. PMID: 11148253
93. Lesne S, Koh MT, Kotilinek L, Kayed R, Glabe CG, Yang A, et al. A specific amyloid-beta protein assembly in the brain impairs memory. *Nature*, 2006; 440(7082):352–7. <https://doi.org/10.1038/nature04533> PMID: 16541076
94. Borbely E, Horvath J, Furdan S, Bozso Z, Penke B, Fulop L. Simultaneous changes of spatial memory and spine density after intrahippocampal administration of fibrillar abeta1–42 to the rat brain. *Biomed Res Int*, 2014; 2014: 345305. <https://doi.org/10.1155/2014/345305> PMID: 25050342
95. Heredia L, Helguera P, de Olmos S, Kedikian G, Sola Vigo F, LaFerla F, et al. Phosphorylation of actin-depolymerizing factor/cofilin by LIM-kinase mediates amyloid beta-induced degeneration: a potential mechanism of neuronal dystrophy in Alzheimer's disease. *J Neurosci*, 2006; 26(24):6533–42. <https://doi.org/10.1523/JNEUROSCI.5567-05.2006> PMID: 16775141
96. Lacor PN, Buniel MC, Furlow PW, Clemente AS, Velasco PT, Wood M, et al. Abeta oligomer-induced aberrations in synapse composition, shape, and density provide a molecular basis for loss of

- connectivity in Alzheimer's disease. *J Neurosci*, 2007; 27(4):796–807. <https://doi.org/10.1523/JNEUROSCI.3501-06.2007> PMID: 17251419
97. Hardy J.A. and Higgins G.A. Alzheimer's disease: the amyloid cascade hypothesis. *Science*, 1992; 256(5054):184–5. PMID: 1566067
98. Selkoe D.J. Alzheimer's disease is a synaptic failure. *Science*, 2002; 298(5594):789–91. <https://doi.org/10.1126/science.1074069> PMID: 12399581
99. Tackenberg C. and Brandt R. Divergent pathways mediate spine alterations and cell death induced by amyloid-beta, wild-type tau, and R406W tau. *J Neurosci*, 2009; 29(46):14439–50. <https://doi.org/10.1523/JNEUROSCI.3590-09.2009> PMID: 19923278
100. Baj G, Patrizio A, Montalbano A, Sciancalepore M, Tongiorgi E. Developmental and maintenance defects in Rett syndrome neurons identified by a new mouse staging system in vitro. *Front Cell Neurosci*, 2014; 8:18. <https://doi.org/10.3389/fncel.2014.00018> PMID: 24550777
101. Tatavarty V, Kim EJ, Rodionov V, Yu J. Investigating sub-spine actin dynamics in rat hippocampal neurons with super-resolution optical imaging. *PLoS One*, 2009; 4(11):e7724. <https://doi.org/10.1371/journal.pone.0007724> PMID: 19898630
102. Harris K.M., Jensen F.E., and Tsao B. Three-dimensional structure of dendritic spines and synapses in rat hippocampus (CA1) at postnatal day 15 and adult ages: implications for the maturation of synaptic physiology and long-term potentiation. *J Neurosci*, 1992; 12(7):2685–705 PMID: 1613552
103. Etienne-Manneville S. and Hall A. Rho GTPases in cell biology. *Nature*, 2002; 420(6916): 629–35. <https://doi.org/10.1038/nature01148> PMID: 12478284
104. Schubert V. and Dotti C.G. Transmitting on actin: synaptic control of dendritic architecture. *J Cell Sci*, 2007; 120(Pt 2):205–12. <https://doi.org/10.1242/jcs.03837> PMID: 17215449
105. Tada T. and Sheng M. Molecular mechanisms of dendritic spine morphogenesis. *Curr Opin Neurobiol*, 2006; 16(1):95–101. <https://doi.org/10.1016/j.conb.2005.12.001> PMID: 16361095
106. Mizuno K.. Signaling mechanisms and functional roles of cofilin phosphorylation and dephosphorylation. *Cell Signal*, 2013; 25(2):457–69. <https://doi.org/10.1016/j.cellsig.2012.11.001> PMID: 23153585
107. Bamburg J.R. Proteins of the ADF/cofilin family: essential regulators of actin dynamics. *Annu Rev Cell Dev Biol*, 1999; 15:185–230. <https://doi.org/10.1146/annurev.cellbio.15.1.185> PMID: 10611961
108. Mendoza-Naranjo A, Contreras-Vallejos E, Henriquez DR, Otth C, Bamburg JR, Macchioni RB, et al. Fibrillar amyloid-beta1-42 modifies actin organization affecting the cofilin phosphorylation state: a role for Rac1/cdc42 effector proteins and the slingshot phosphatase. *J Alzheimers Dis*, 2012; 29(1):63–77. <https://doi.org/10.3233/JAD-2012-101575> PMID: 22204905
109. Minamide LS, Striegl AM, Boyle JA, Meberg PJ, Bamburg JR. Neurodegenerative stimuli induce persistent ADF/cofilin-actin rods that disrupt distal neurite function. *Nat Cell Biol*, 2000; 2(9):628–36. <https://doi.org/10.1038/35023579> PMID: 10980704
110. Woo JA, Jung AR, Lakshmana MK, Bedrossian A, Lim Y, Bu JH, et al. Pivotal role of the RanBP9-cofilin pathway in Abeta-induced apoptosis and neurodegeneration. *Cell Death Differ*, 2012; 19(9):1413–23. <https://doi.org/10.1038/cdd.2012.14> PMID: 22361682
111. Zhao L, Ma QL, Calon F, Harris-White ME, Yang F, Lim GP, et al. Role of p21-activated kinase pathway defects in the cognitive deficits of Alzheimer disease. *Nat Neurosci*, 2006; 9(2):234–42. <https://doi.org/10.1038/nn1630> PMID: 16415866
112. Bellenchi GC, Gurniak CB, Perlas E, Middei S, Ammassari-Teule M, Witke W. N-cofilin is associated with neuronal migration disorders and cell cycle control in the cerebral cortex. *Genes Dev*, 2007; 21(18): 2347–57. <https://doi.org/10.1101/gad.434307> PMID: 17875668
113. Ma QL, Yang F, Calon F, Ubeda OJ, Hansen JE, Weisbart RH, et al. p21-activated kinase-aberrant activation and translocation in Alzheimer disease pathogenesis. *J Biol Chem*, 2008; 283(20):14132–43. <https://doi.org/10.1074/jbc.M708034200> PMID: 18347024
114. Morishita W., Marie H., and Malenka R.C. Distinct triggering and expression mechanisms underlie LTD of AMPA and NMDA synaptic responses. *Nat Neurosci*, 2005; 8(8): 1043–50. <https://doi.org/10.1038/nn1506> PMID: 16025109
115. Wang Y, Dong Q, Xu XF, Feng X, Xin J, Wang DD, et al. Phosphorylation of cofilin regulates extinction of conditioned aversive memory via AMPAR trafficking. *J Neurosci*, 2013; 33(15):6423–33. <https://doi.org/10.1523/JNEUROSCI.5107-12.2013> PMID: 23575840
116. Yuen EY, Liu W, Kafri T, van Praag H, Yan Z. Regulation of AMPA receptor channels and synaptic plasticity by cofilin phosphatase Slingshot in cortical neurons. *J Physiol*, 2010; 588(Pt 13):2361–71. <https://doi.org/10.1113/jphysiol.2009.186353> PMID: 20442266
117. Barone E., Mosser S., and Fraering P.C. Inactivation of brain Cofilin-1 by age, Alzheimer's disease and gamma-secretase. *Biochim Biophys Acta*, 2014; 1842(12 Pt A):2500–9. <https://doi.org/10.1016/j.bbadi.2014.10.004> PMID: 25315299

118. Song X, Chen X, Yamaguchi H, Mouneimne G, Condeelis JS, Eddy RJ. Initiation of cofilin activity in response to EGF is uncoupled from cofilin phosphorylation and dephosphorylation in carcinoma cells. *J Cell Sci*, 2006; 119(Pt 14):2871–81. <https://doi.org/10.1242/jcs.03017> PMID: 16803871
119. Bravo-Cordero JJ, Oser M, Chen X, Eddy R, Hodgson L, Condeelis J. A novel spatiotemporal RhoC activation pathway locally regulates cofilin activity at invadopodia. *Curr Biol*, 2011; 21(8): 635–44. <https://doi.org/10.1016/j.cub.2011.03.039> PMID: 21474314
120. Tania N, Prost E, Condeelis J, Edelstein-Keshet L. A temporal model of cofilin regulation and the early peak of actin barbed ends in invasive tumor cells. *Biophys J*, 2011; 100(8): p. 1883–92. <https://doi.org/10.1016/j.bpj.2011.02.036> PMID: 21504724
121. Hsieh H, Boehm J, Sato C, Iwatsubo T, Tomita T, Sisodia S, et al. AMPAR removal underlies Abeta-induced synaptic depression and dendritic spine loss. *Neuron*, 2006; 52(5): p. 831–43. <https://doi.org/10.1016/j.neuron.2006.10.035> PMID: 17145504
122. Burridge K. and Wennerberg K. Rho and Rac take center stage. *Cell*, 2004; 116(2):167–79. PMID: 14744429
123. Jaffe A.B. and Hall A. Rho GTPases: biochemistry and biology. *Annu Rev Cell Dev Biol*, 2005; 21:247–69. <https://doi.org/10.1146/annurev.cellbio.21.020604.150721> PMID: 16212495
124. Parri M. and Chiarugi P. Rac and Rho GTPases in cancer cell motility control. *Cell Commun Signal*, 2010; 8:23. <https://doi.org/10.1186/1478-811X-8-23> PMID: 20822528
125. Ridley AJ, Schwartz MA, Burridge K, Firtel RA, Ginsberg MH, Borisy G, et al. Cell migration: integrating signals from front to back. *Science*, 2003; 302(5651):1704–9. <https://doi.org/10.1126/science.1092053> PMID: 14657486
126. Takai Y., Sasaki T., and Matozaki T. Small GTP-binding proteins. *Physiol Rev*, 2001; 81(1):153–208. PMID: 11152757
127. Byrne KM, Monsefi N, Dawson JC, Degasperi A, Bukowski-Wills JC, Volinsky N, et al. Bistability in the Rac1, PAK, and RhoA Signalling Network Drives Actin Cytoskeleton Dynamics and Cell Motility Switches. *Cell Syst*, 2016; 2(1):38–48. <https://doi.org/10.1016/j.cels.2016.01.003> PMID: 27136688
128. Cichon J, Sun C, Chen B, Jiang M, Chen XA, Sun Y, et al. Cofilin Aggregation Blocks Intracellular Trafficking and Induces Synaptic Loss in Hippocampal Neurons. *Journal of Biological Chemistry*, 2011; 287(6):3919–3929 <https://doi.org/10.1074/jbc.M111.301911> PMID: 22184127